Coordination Chemistry Reviews 419 (2020) 213397

Contents lists available at ScienceDirect

Coordination Chemistry Reviews

journal homepage: www.elsevier.com/locate/ccr

Review

Role of oxidation state, ferryl-oxygen, and ligand architecture on the reactivity of popular high-valent Fe^{IV}=O species: A theoretical perspective

Ravi Kumar, Bhawana Pandey, Asmita Sen, Mursaleem Ansari, Sunita Sharma, Gopalan Rajaraman *

Department of Chemistry, Indian Institute of Technology Bombay, Powai, Mumbai 400076, India

ARTICLE INFO

Article history:
Received 9 August 2019
Received in revised form 9 March 2020
Accepted 11 May 2020
Available online 28 May 2020

ABSTRACT

High-valent iron-oxo species are ubiquitous in nature and are present at the active site of several metalloenzymes which perform challenging organic transformations. Mimicking these metalloenzyme reactivities is one of the growing areas of research, and over the last two decades, tremendous progress has been made to mimic both the structure and function of various heme and non-heme metalloenzymes. Understanding the mechanism of catalytic reactions of these enzymes and their biomimetic models are extremely important to improvise the models further. However, due to the open-shell nature of the catalyst with often close-lying spin-states, the mechanistic aspects associated are highly complex. In this regard, computational tools have played a pivotal role in underpinning the mechanism and several important concepts such as two-state/multi-state reactivity, exchange-enhanced reactivity has emerged. While there are several reviews written already on the reactivity of the popular high-valent Fe^{IV}=O species, the comparative oxidative ability of this species to other oxidants has not been reviewed. Our group has been working actively in this area, and here we have compared the oxidative ability of the Fe^{IV}=O to other species with variation arising due to (i) oxidation state (ii) ligand architecture (iii) substitution of oxo by the isoelectronic nitrene species. In this review, theoretical studies undertaken in this spirit are summarised to provide birds-eye-view on the reactivity of the popular Fe^{IV}=O species. The facts/concepts discussed here will undoubtedly be helpful to design efficient bioinspired catalysts in the years to come.

Contents

1. Introduction

High-valent heme and non-heme metal-oxo complexes are aggressive and compelling oxidants in various biological processes that occurred in nature [1–19]. Their presence in the active site of metalloenzymes fascinates researchers to study the synthesis, structure of the coordination site, and most importantly, their reactivity [14]. The study of these types of complexes is not only helpful in understanding bio-inorganic chemistry but also very useful in academics and the pharmaceutical/drug industry [20,21]. In recent decades, among all the high-valent metal-oxo complexes, the Fe^{IV}=O species have gained much attention due to their pres-

* Corresponding author at: Department of Chemistry, IIT Bombay, Powai, Mumbai - 400076.
E-mail address: rajaraman@chem.iitb.ac.in (G. Rajaraman).

https://doi.org/10.1016/j.ccr.2020.213397
0010-8545/

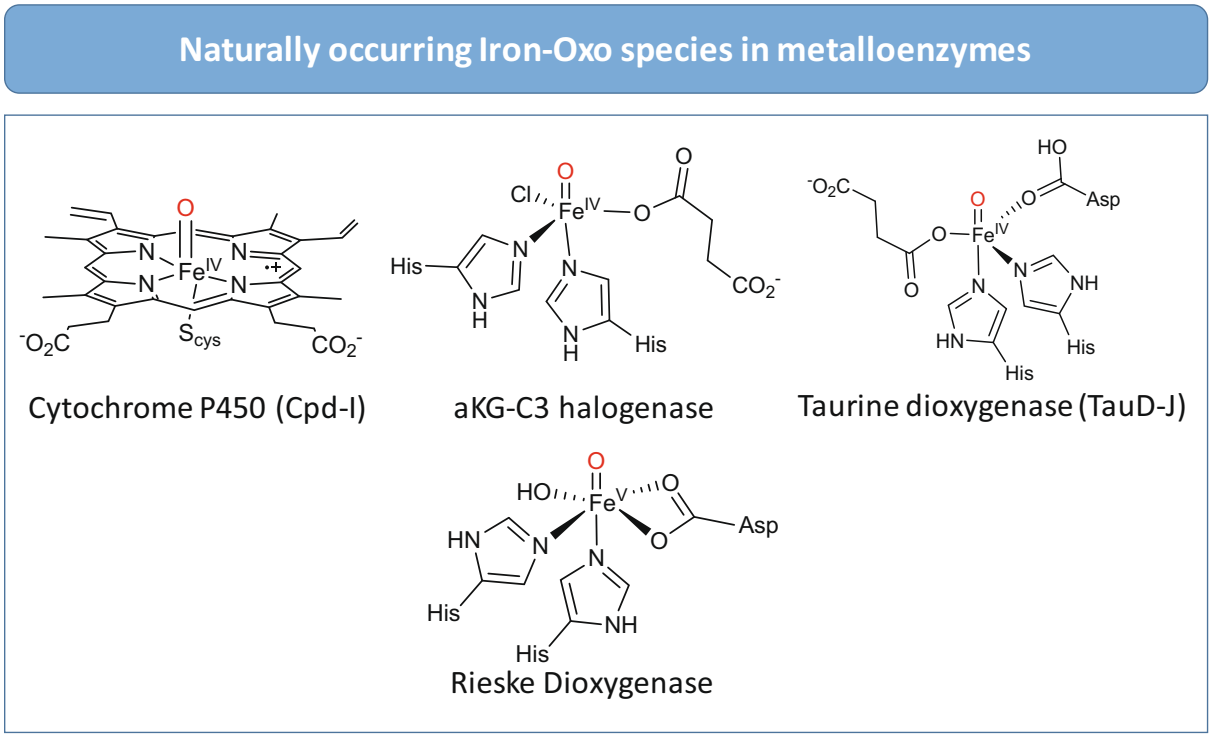

Scheme 1. High-valent Iron-Oxo species in the active site of various heme and non-heme enzymes.

ence in the active site of many of the vital metalloenzymes such as cytochrome P450 (see Scheme 1), a naturally occurring heme metalloenzyme containing iron metal in their active site and best known to catalyse various oxidation reactions in biological systems [3,7,14,16,17]. Due to their strong oxidising ability, heme and non-heme Fe^{IV}=O species are effortlessly good in catalysing many metabolic reactions like dioxygen activation, atom transfer reactions, C–H activation that lead to hydroxylation, epoxidation or halogenation products [14,16,17,22–24]. In 2003, Krebs and co-workers, successfully detected the high spin Fe^{IV}=O species by the Mössbauer and electron paramagnetic resonance (EPR) spectroscopic techniques during the reaction of TauD (taurine αKG dioxygenase, see Scheme 1.) with dioxygen [25]. The spectroscopic characterisation of these cagey species fascinated bio-inorganic chemists to explore the synthesis, characterisation, and reactivity of these species. These species become so popular in the biomimetic chemistry of metalloenzymes where high-valent iron-oxo species were involved [12]. Since the study of these molecules becomes easier than the original metalloenzymes with higher molecular mass, the high-valent Fe^{IV}=O species are reported as a potent oxidant in various chemical reactions [12,26]. There are numerous studies reported to understand the mechanism of oxidation reactions catalysed or mediated by Fe^{IV}=O complexes yielding a mixture of products, and it is often difficult to obtain regio/chemoselectivity with this oxidant. Interestingly, many recent reports shed light on such reactions with high selectivity, for example, *ortho*-hydroxylation [27–31], *ortho*-halogenation reactions [12,32–43], etc. Another important factor in attaining selectivity is ligand design, by simply tuning the ligand architecture one can achieve selectivity with high efficiency [23,44–49]. The activation or functionalization of C–H bond are challenging as this demands a high bond dissociation energy and high-valent oxidant such as the one focused here eases this demand and facilitate these organic transformations.

One of the key development that has happened in this area is of utilising state-of-the-art computing techniques to gain insight into the mechanistic aspect of these species. In fact, DFT calculations have played a prominent role in unveiling the popular "two-state reactivity" concept in simple gaseous Fe^{IV}=O species as early as in 1995 by Shaik and co-workers [50]. While this concept has been expanded to include various cases over the years, the idea formulated suggests that the reactions are not necessarily happening on the ground spin state structure of the reactant. This is exclusively applicable only when the catalyst has unpaired electrons and thus are paramagnetic in nature. If the catalyst is diamagnetic or if the excited states are higher in energy, the reactions are expected to occur at the ground state, and this is termed as single-state reactivity (see Fig. 1a). Even if the spin multiplicity of the reactant and the products are the same, the barrier height of the transition state of the other spin states decides whether a particular reaction follows a two-state reactivity or not. In simple terms, this means that the reactivity is controlled by more than one spin state and spin-crossover from one spin surface to the other during the course of the reactions is thus expected. Depending on the spin state of the reactant and the product, there can be one or many spin-crossover during the course of the reactions (see Fig. 1b). If more than two-spin states are present for the reactant or even the intermediates that form during the course of the reaction, then the reaction can happen in different spin-surfaces leading to the proposal of multi-state reactivity wherein more than two-spin state decides the course of the reactions (see Fig. 1c). Ever since this concept was proposed, the application of the same in this chemistry is imminent, and over the years computational techniques played an important role in understanding the reactivity of these elusive species and several conceptual advancements have been made to achieve the predictive power in terms of ligand design. These advancement has been reviewed already by Shaik and co-workers [17].

In our current review, we intend to focus our attention on the importance of the structure on the reactivity of non-heme Fe^{IV}=O species specifically towards C–H bond activation reactions and particularly how different ligand design enable higher reactivity.

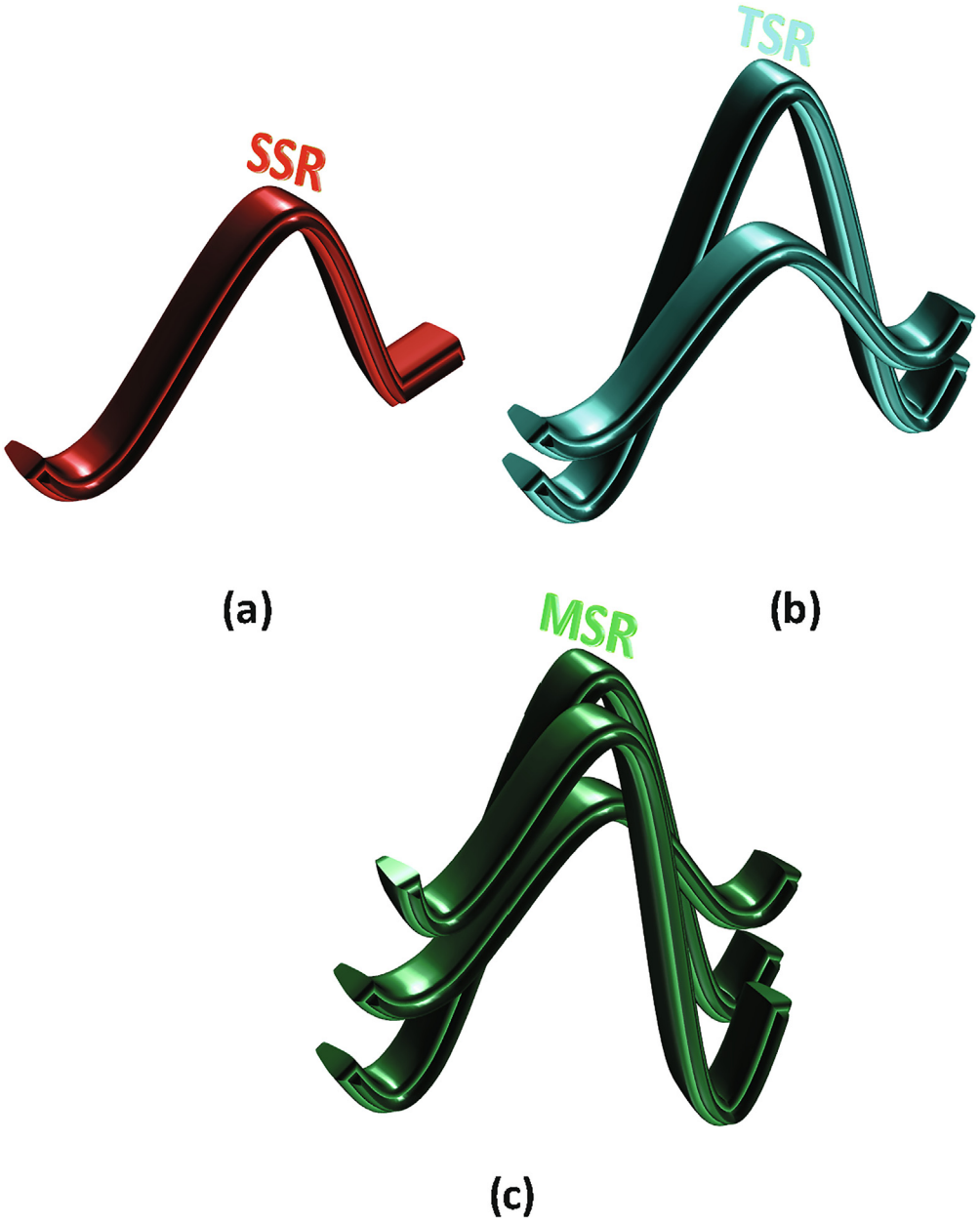

Fig. 1. Schematic representation for (a) single-state reactivity (SSR) (b) two-state reactivity (TSR) and (c) multi-state reactivity (MSR).

Later, we have expanded the scope of the review to cover other relevant high-valent species such as *iso*-electronic Fe^{IV}=NTs species which are known to perform similar functions like *ortho*-amination to understand better the electronic structure and reactivity of both the species. In the first part of the current review, we focus our attention on various factors that control the reactivity of high-valent Fe^{IV}=O species. The most important one being, how comparable the oxidative abilities of different redox states belong to iron-oxo wherein a larger oxidation state has been proposed to enhance the reactivity [27,30]. The next important comparison for the reactivity of Fe^{IV}=O species resides on comparing its reactivity to its precursor materials such as Fe^{III}-OOH species when generated using H_2O_2 or Fe^{III}-OIPh species from iodosylarene. After this, we intend to diversify on how important the equatorial ligands are, in controlling the reactivity of Fe^{IV}=O species? This will be followed by the importance of the ligand design to enhance the reactivity of Fe^{IV}=O towards industrially relevant yet challenging reactions such as enantioselective halogenation/nitration of aliphatic and aromatic compounds. Finally, to see if replacing ferryl-oxo by isoelectronic nitrene would enhance the reactivity, we have compared the reactivity of Fe^{IV}=O species with isoelectronic Fe^{IV}=NTs species with various ligand architecture to conclude the mononuclear iron-oxo section.

2. Reactivity of various redox states of high-valent Iron-Oxo species

The Fe^{IV}=O species is an invincible oxidant; however, the prediction of the correct oxidation state in metalloenzymes is always a contentious issue. Among various high-valent Fe^{n+}=O species (n = 3, 4 or 5), there is still controversy regarding the oxidation states whether the reaction is going via a high-valent intermediate such as Fe^{IV}=O, Fe^{V}=O or directly via Fe^{III}-OX adducts (where X = IPh, OH, OR, halides). While different reactions and reaction

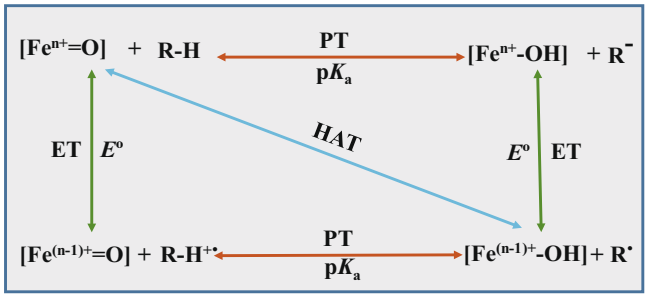

Fig. 2. Schematic representation of the thermodynamic relationship of reduction potential (E°) and acidity constants (pK_a) where ET and PT correspond to electron transfer and proton transfer, respectively.

conditions favour different oxidation states and oxidant, to assess the comparative oxidative ability of these oxidants, only prototype reaction needs to be chosen. In this regard, Neese and our group have performed some theoretical studies. Neese and co-workers have modelled the *hexa*-coordinated complexes of $Fe^{IV/V/IV}$=O with small ligands such as 4-NH_3 at equatorial and 1-OH at an axial position to Fe^{n+}=O moiety [51]. The computational studies on these modelled complexes revealed an enhancement in the reactivity with the increase in oxidation states which lead to a decrease in barrier height for C–H activation (69.7 kJ/mol for Fe^{IV}=O, 16.8 kJ/mol for Fe^{V}=O and barrierless for Fe^{VI}=O). As we know that the increase in oxidation state increases the tendency to accept electrons which means an enhancement in the electrophilicity of metal. In case of above modelled iron-oxo complexes, the decrease in the barrier height is rationalise based on two factors; 1) the increase in electrophilicity of Fe^{n+}=O and 2) the $Fe^{(n-1)+}$–OH formed after the transfer of hydrogen from the substrate to Fe^{n+}=O, increases the bond dissociation energy (BDE) of O–H. Basically, the BDE is a thermodynamic force to understand the reactivity of hydrogen atom transfer (HAT) reactions. It is given by the difference between BDE of substrate C–H bond and BDE of FeO-H bond formed after H transfer. Mayer [52] has popularized this in terms of reduction potential (E°) and acidity constants (pK_a), using a simple thermodynamic cycle (see Fig. 2) and expressed as Eq. (1) given below.

$$BDE = 1.37pKa + 23.06E^{\circ} + C \quad (1)$$

Here, C is a solvent dependent correction factor. BDE also plays an important role to understand the effect of ligands on reactivity.

Apart from understanding the reactivity of various redox states using fictitious models, calculations have also been performed on experimentally reported bio-mimic systems focusing on the relative reactivity of various iron-oxo redox states. The example that we would like to discuss here is the conversion of benzoic acid to salicylic acid in the presence of hydrogen peroxide using Fe^{III}-OOH/Fe^{IV}=O and Fe^{V}=O species (see Scheme 2) [27,30].

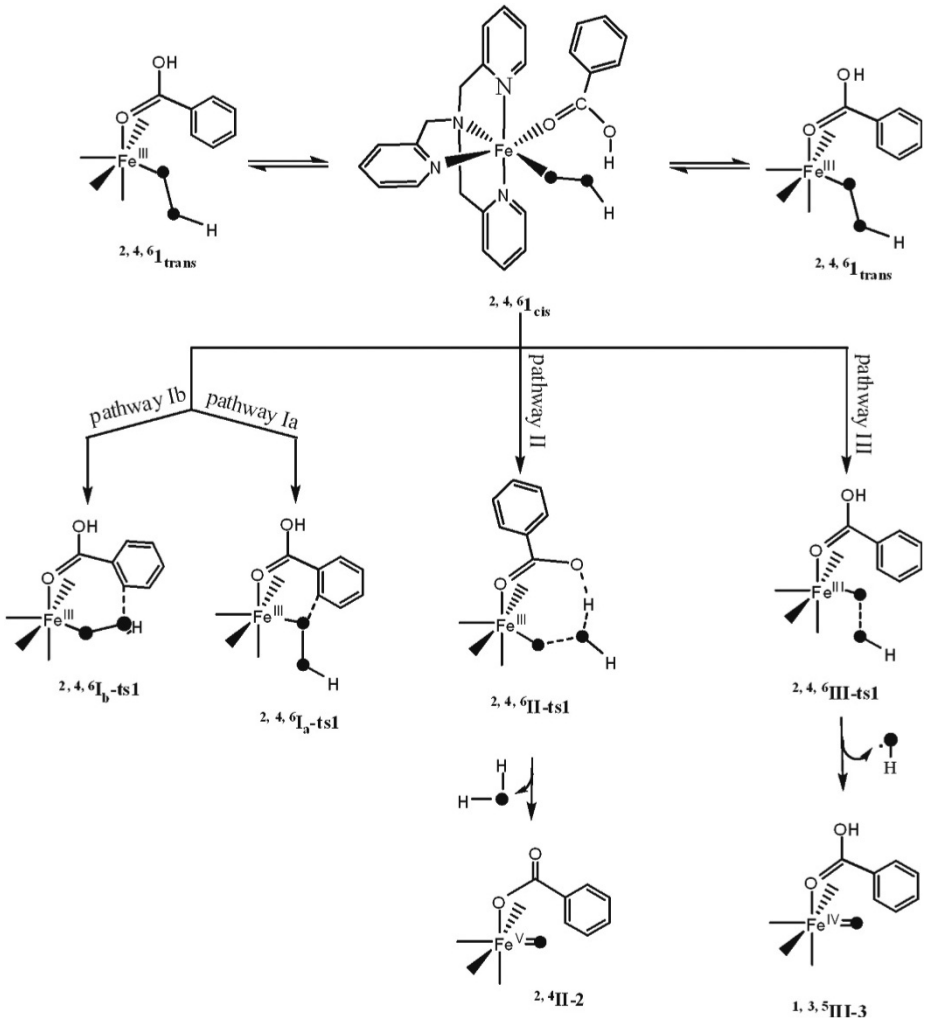

Scheme 2. Schematic representation of various possible pathways occurs in aromatic compounds *ortho*-hydroxylation with iron complexes. Reprinted (adapted) with permission from Ref. [27]. Copyright (2013) American Chemical Society.

The schematic pathway that is adapted for the DFT calculation is shown in Scheme 2. Here pathway I represent, Fe^{III}-OOH as the potent oxidant, considering both the distal and proximal oxygen atom for the *ortho*-hydroxylation. Pathway II and III represent hetero and homolytic cleavage of the O···O bond yielding aggressive Fe^{V}=O and Fe^{IV}=O oxidant, respectively. Particularly, the heterolytic cleavage of the O···O bond is assumed to take place by the acid assisted cleavage (cis form) while the homolytic cleavage takes place in the *trans*-form. The barrier height for the first transition state in pathway Ia with distance and proximal oxygen atoms at the sextet spin surface was found to be 115.8 and 154.0 kJ/mol, respectively. These barriers are much higher than the O···O cleavage and the barriers associated with the attack of the generated high-valent oxidant on the substrate; hence the possibility of Fe^{III}-OOH as a possible oxidant in this chemistry is ruled out. This also sheds light on the need to evoke such high-valent oxidants in this chemistry. Pathway II considers the formation of Fe^{V}=O species via the heterolytic cleavage of O···O bond with a cis form of acid. To clearly estimate the comparative oxidative ability, it is also important to consider the barrier height associated with the attack of Fe^{V}=O on the substrate. Here two different pathways were considered with the first one involving C–H bond activation of aromatic compound and the second one considering the electrophilic attack of the ferryl oxygen directly on the aromatic ring (see Scheme 3) and the estimated barrier for these were 45.5 and 5.4 kJ/mol, respectively. This reveals that the electrophilic attack is favoured and the overall barrier for the hydroxylation is still small compared to the Fe^{III}-OOH as the oxidant. Pathway III involves the formation of Fe^{IV}=O intermediate with a barrier height needed for the cleavage of O···O bond to be 109.6, 123.7 and 126.3 kJ/mol for the sextet, doublet and the quartet states, respectively. Here as well the energy required for further oxidation is computed, and the electrophilic attack of Fe^{IV}=O on the aromatic ring is again favoured with an estimated barrier of 71.6 kJ/mol (vs. 115.7 kJ/mol for the C–H bond activation). Comparatively, not only the formation of Fe^{V}=O is favoured in this case (see Fig. 3), the barrier needs for activating the substrate is also much lower for the Fe^{V}=O compared to Fe^{IV}=O species. This unequivocally suggests Fe^{V}=O as the potent oxidant in this chemistry.

Further, the effect of different ligand environments on the *ortho*-hydroxylation reaction has been explored using $[(BPMEN)(PhCOO)Fe^{V}=O]^{2+}$ and $[(TPA)(PhCOO)Fe^{V}=O]^{2+}$ species [30]. Experimental findings suggest that $[(BPMEN)(CH_3CN)_2Fe^{II}]^{2+}$ being more reactive than $[(TPA)(CH_3CN)_2Fe^{II}]^{2+}$complex [29,31].

The complexes $[(BPMEN)(C_6H_5COO)Fe^{V}=O]^{2+}$ and $[(TPA)(C_6H_5COO)Fe^{V}=O]^{2+}$ have doublet spin (S = 1/2) as a ground state. Looking into the electronic structure of these two complexes, the BPMEN has two pyridine rings, one is parallel and another one perpendicular to the Fe=O bond (see Scheme 4). While in the case of TPA ligand complex, two of the three rings are located parallel to the Fe=O bond, leaving one residing perpendicular to the bond (see Scheme 4). This could be the main reason to attribute the reactivity differences between the two species. To investigate further depending on the orientation of the pyridine ring with respect to Fe=O bond, all the three possible isomers of the complex $[(BPMEN)(C_6H_5COO)Fe^{V}=O]^{2+}$ viz. regular, ring aligned parallel and ring situated perpendicular to Fe=O have been calculated. This reveals that the Fe-N distances are slightly larger when rings orienting parallel leads mixing between the π-orbitals of the pyridine and $(\pi_{Fe(dyz)-O(py)})^{*}$ orbital of the Fe=O moiety.

The comparative energy landscape computed for the *ortho*-hydroxylation reaction by the complex $[(BPMEN)(C_6H_5COO)Fe^{V}=O]^{2+}$ and $[(TPA)(C_6H_5COO)Fe^{V}=O]^{2+}$ has been shown in the Fig. 4. From potential energy surface, it is evident that O···O bond cleavage is facile in TPA ligand complex than that of in BPMEN ligand complex (0.9 vs. 73.6 kJ/mol, see Fig. 4). The rate-determining step

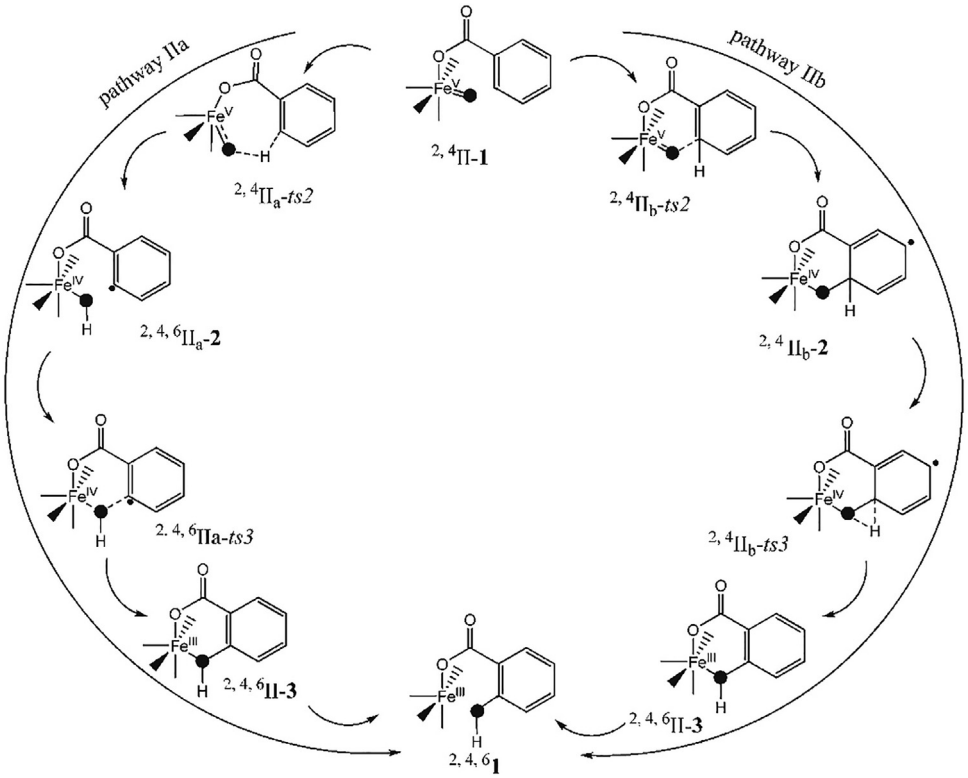

Scheme 3. Mechanistic representation of *ortho*-hydroxylation using Fe^{V}=O species. Reprinted (adapted) with permission from Ref. [27]. Copyright (2013) American Chemical Society.

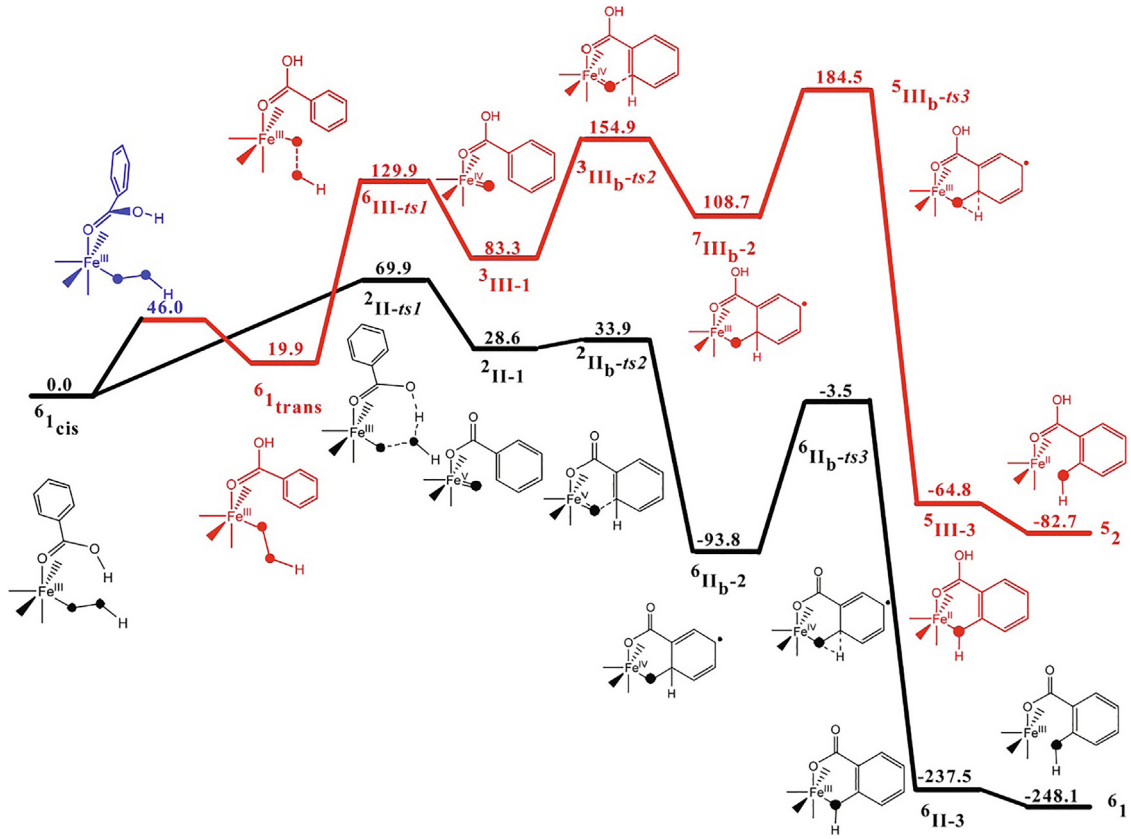

Fig. 3. A comparative study between Fe^{IV}=O (red) and Fe^{V}=O(black) species in aromatic *ortho*-hydroxylation. All energies were given in kJ/mol. Reprinted (adapted) with permission from Ref. [27]. Copyright (2013) American Chemical Society.

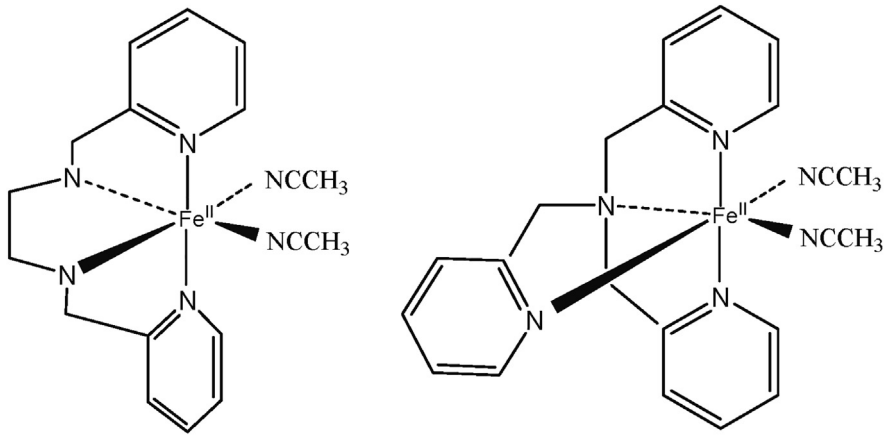

Scheme 4. A schematic diagram of the core geometries of $[(BPMEN)(CH_3CN)_2Fe^{II}]^{2+}$ and $[(TPA)(CH_3CN)_2Fe^{II}]^{2+}$. Reprinted (adapted) with permission from Ref. [30]. Copyright (2014) The Royal Society of Chemistry.

i.e. electrophilic attack on the aromatic ring shows a slightly lower barrier (2.7 kJ/mol) for $[(BPMEN)(C_6H_5COO)Fe^{V}=O]^{2+}$ than that calculated for the $[(TPA)(C_6H_5COO)Fe^{V}=O]^{2+}$ (5.3 kJ/mol), this confirms the faster reactivity of the BPMEN compared to TPA and these findings are in agreement with experiments.

In 2002, Que and co-workers reported reactivity studies on $[(TPA)Fe^{II}(CH_3CN)_2]^{2+}$ complex using DFT calculation by generating a high-valent species [53]. For this complex, stereospecific hydrocarbon oxidation was reported when it reacts with H_2O_2. From experimental observations, the participation of $HO^{\bullet}$ in the reaction was discarded due to the stereoselectivity of the reaction. Only probable species i.e. Fe^{III}-OOH, Fe^{IV}=O, and Fe^{V}=O are left to consider that can trigger this reaction. In this work, the authors propose water-assisted heterolytic cleavage to form *cis*-HO-Fe^{V}=O oxidant. The computed barrier heights for homo and heterolytic O-O bond cleavage found to be comparable, but the formation of Fe^{IV}=O came out to be highly endothermic compared to Fe^{V}=O (see Fig. 5). They have simultaneously performed the calculations on $[(TPA)Fe^{III}$-OOR] (R = CH_3) species which revealed that the Fe^{IV}=O and Fe^{V}=O intermediate generated through homolytic and het-

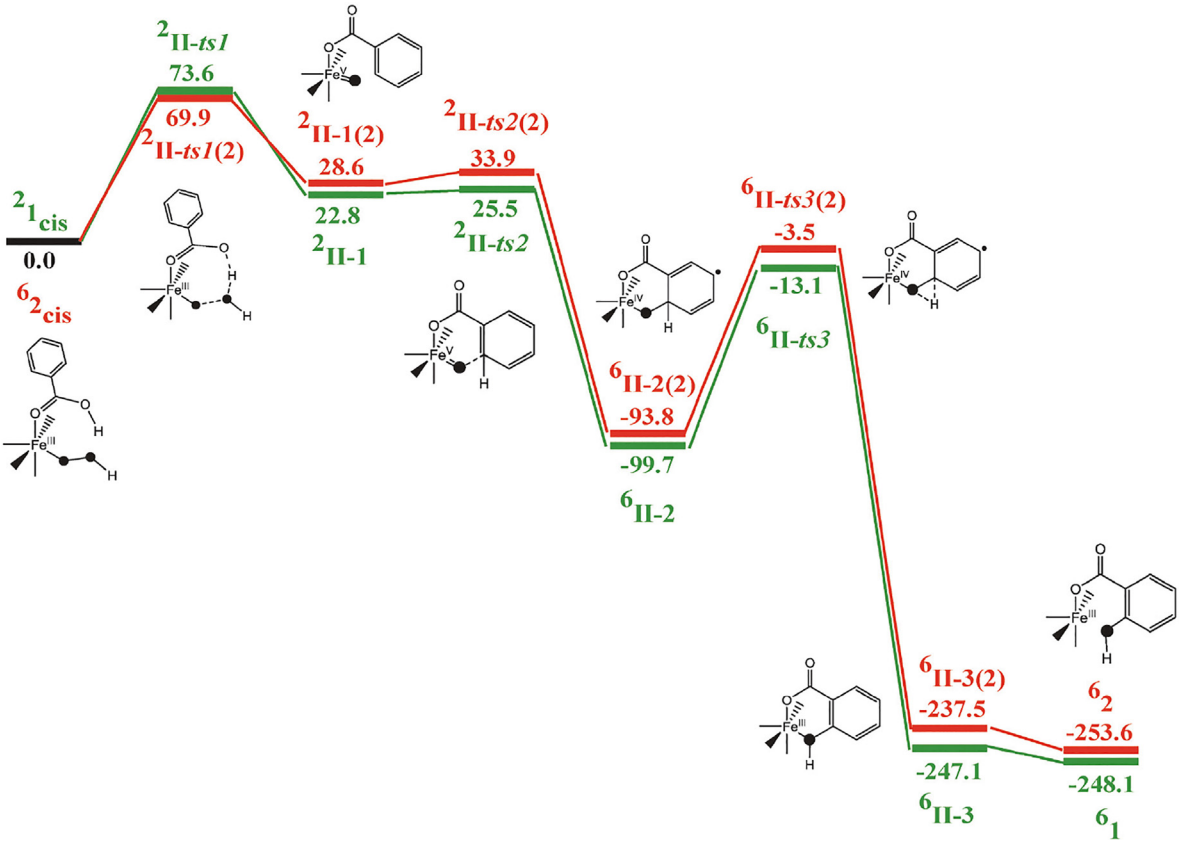

Fig. 4. A comparative potential energy surface (ΔG in kJ/mol) between Fe^{V}=O species containing BPMEN (green) and TPA (red) ligand architecture. All energies are in kJ /mol. Reprinted (adapted) with permission from Ref. [30]. Copyright (2014) The Royal Society of Chemistry.

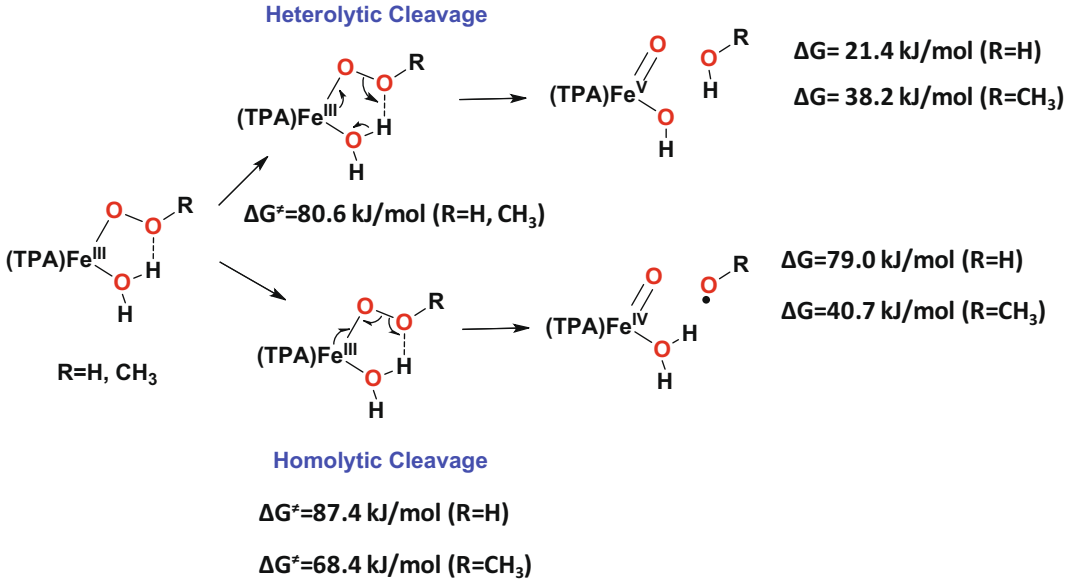

Fig. 5. Schematic representation of water-assisted homolytic and heterolytic cleavage of Fe^{III}-OOR(R = H, CH_3) moiety.

erolytic O-O bond cleavage was almost degenerate and barrier height for the homolytic cleavage was found to be lower than that of Fe^{III}-OOH (see Fig. 5). These two observations led them to conclude that the Fe^{III}-OOH prefers the heterolytic cleavage while Fe^{III}-OOR follows homolytic pathways explaining all the experimental data.

In the above paragraph, we have discussed the modification in the oxidant moiety from –OOH to –OOR leads to different reactive species formation. Here, we will be going to discuss the spin-state energetics change with the ligand attached to the iron center. Shaik and co-workers studied the Fe^{V}=O species using coupled cluster CCSD(T) and DFT calculations [54]. This study gives us an idea

about ligands present around Fe^{V}=O moiety if a σ-donor amine or pyridine ligands are present and not a –OH or –OR (π-donor ligands) group. In these circumstances, S = 3/2 (quartet) and S = 1/2 (doublet) energy gaps are small with doublet being the ground state. One more interesting finding from this study is that when a π-donor ligand is cis to Fe^{V}=O, the quartet state becomes the ground state while π-donor ligand trans to Fe^{V}=O stabilise a doublet ground state.

Most often, the stable Fe^{V}=O complexes belong to the tetraamido macrocyclic ligand (TAML) group [55–58]. Here, the tetra-anionic amido $TAML^{4-}$ neutralize the high positive charge of Fe^{V}=O moiety offering stability to these species (see Fig. 6). A comparison among Fe^{V}=O and Fe^{IV}=O moiety with this ligand suggests higher reactivity for Fe^{V}=O, as stated earlier [51]. Modification of TAML ligand with biuret group leads to the formation of room temperature stable Fe^{V}=O species (see Fig. 6) [58]. Due to the high electrophilicity of Fe^{V}=O moiety, it also oxidises the strong C–H bond of cyclohexane [56] as well as styrene C=C bond [57], which is consistent with theory and experimental observations reported. The above modification in TAML ligand reduces the HAT reactivity due to high charge delocalisation which increases the electron donation efficiency and results in decreased redox potential. The replacement of tetra-anionic amido ligand with a neutral ligand such as $PyNMe_3$, further increases the reactivity of Fe^{V}=O core [59,60]. This enhanced reactivity was rationalised based on the difference in electrophilicity of the Fe^{V}=O moiety due to the difference in the strength/charges on the equatorial ligands. These oxidants are found to be extraordinary oxidants for C–H bond activation.

Oxidative abilities of high-valent iron-oxo species are well established. However, very little is known about the oxidative abilities of the precursor complexes that generate these species. For example, $LFe^{II/III}$-OIPh is often utilised to generate LFe^{IV}=O/LFe^{V}=O species exclusively. However, often these conversions are not 100% leading to the coexistence of the catalytic precursor in the solution. Given this background, it is important to establish the comparative oxidative ability of the precursor materials vis-à-vis $Fe^{IV/V}$=O species. In this part of the review, we aim to compare the oxidative abilities of high-valent metal-oxo species vis-à-vis their precursors such as Fe^{III}-OX (where X = IPh, OH and OR).

There are only a few thorough experimental studies reported where the comparative oxidative abilities of iodosylarene to $Fe^{IV/V}$=O are compared (see Fig. 7). First, a detailed study has been carried out by Shaik and co-workers [61] in 2007, where their focus was to find the difference between the Cpd I generated with PhIO and other oxidants. Experimental report by Guengerich et al. [62] revealed one of the important facts that the kinetic isotopic effect (KIE) value of Cpd I generated through PhIO gave higher KIE value than that of the natively generated Cpd I which was the starting point to this work. The kinetic barrier for the transfer of oxygen from PhIO to Cpd I was found to be very small in the range of 21.4–33.2 kJ/mol which is lower than the breaking of O-O bond during oxygen atom transfer (42.0–63.0 kJ/mol). The native route follows the doublet spin state (low KIE) while the PhIO route follows a quartet spin state (high KIE). This suggests that the oxygen transfer from PhIO is much faster than that of other oxidants here. From these studies, they have concluded that the high KIE value follows spin-selection rules.

After the report of well-characterized hepta-coordinated complex of Fe^{III}-iodosylarene $[Fe^{III}(tpena)OIPh]^{2+}$ (tpena = N,N,N'-tris(2-pyridylmethyl)ethylenediamine-N'-acetate) from McKenzie and co-workers [63,64] a new era of iodosylarene involvement or form high-valent iron-oxo species came into the picture.

$$LFe^{n+} - OIPh \rightleftharpoons LFe^{(n+2)+} = O + IPh \quad (2)$$

To explore more about the chemistry of iron-iodosylarene (LFe^{n+}-OIPh) precursor compared to high-valent iron-oxo ($LFe^{(n+2)+}$=O) (see the equilibrium of these species in equation (2)), recently, Nam and co-workers published theoretical studies on thioanisole oxidation study with this hepta-coordinated com-

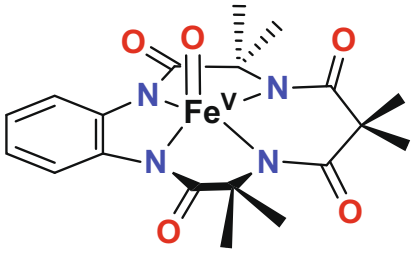

$[(TAML)Fe^{V}=O]^{-}$

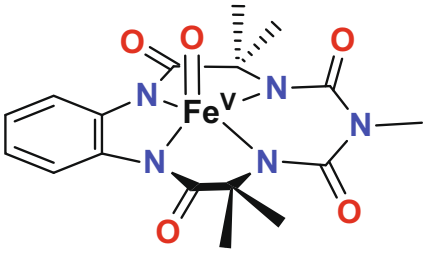

$[(Biuret\ modified\text{-}TAML)Fe^{V}=O]^{-}$

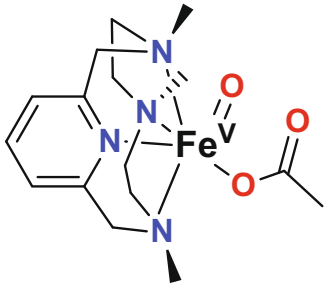

$[(PyNMe_3)(OAc)Fe^{V}=O]^{2+}$

Fig. 6. The structures of well characterized non-heme Fe^{V}=O complexes.

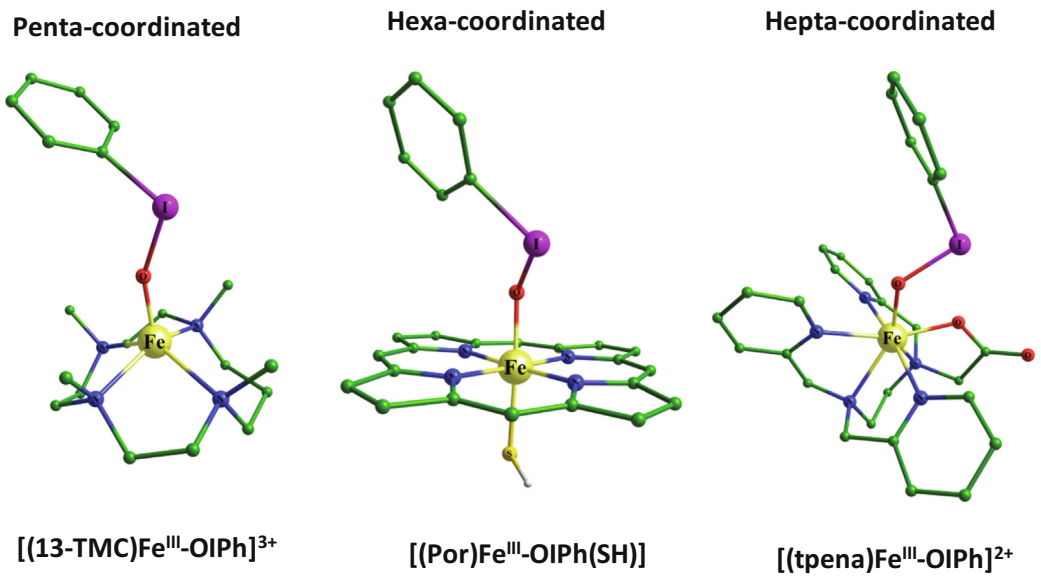

Fig. 7. The geometry of iron(III)-iodosylarene complexes reported in the literature.

plex [65]. The proposed mechanism is shown in Scheme 5. A metal-iodosylarene complex which undergoes O-I bond cleavage at a faster rate to form a high-valent Fe^{IV}=O species. Otherwise, the O-I bond directly acts as an oxidising agent as it has enough oxidising power. But the interesting fact is that this direct attack of substrate-induces two resonance valence-bond structures which leads to product formation.

The theoretical studies on this complex suggested the barrier height to form the Fe^{IV}=O from Fe^{III}-iodosylarene to be 102.9 kJ/-mol, and hence the formation of high-valent species was both kinetically and thermodynamically not feasible (see Scheme 5). Direct oxygen atom transfer reaction expected to occur via two mechanisms; (i) bond-cleavage coupled electron transfer (BCCET) and (ii) direct oxygen-atom transfer (DOT) through Fe^{III}-iodosylarene. BCCET pathway was found to have a barrier height of 81.5 kJ/mol followed by the oxygen atom transfer (OT) barrier height of 2.9 kJ/mol (see Scheme 5). Although the DOT pathway (through the reference point of halogen-bonding reaction complex, **^{6}RC**) was found to have a barrier height of 78.5 kJ/mol, it has been reported to be comparable with BCCET pathway (see Scheme 5). If we consider the reference point to be sextet state of thioanisole oriented toward the oxygen, **^{6}RC**, then the barrier height would be 61.3 kJ/mol. The direct oxygen atom transfers from monomeric iodosylarene were reported to be only 46.2 kJ/mol, which suggested that monomeric iodosylarene is a robust oxidant, but the polymeric structure makes it less reactive. They have calculated the bond dissociation energy for Fe-OIPh bond, which gave an overall barrier to be 113.4 kJ/mol. From these studies, they have concluded that this [Fe^{III}(tpena)OIPh]$^{2+}$ complex can form two resonance valence-bond structure [PhIO···Fe(tpena)] and [PhI···O=Fe(tpena)] in thioanisole sulfoxidation mechanism.

Nam and co-workers reported the experimental studies on the reactivity of high-valent Fe$^{IV/V}$=O in comparison to Fe^{III}-iodosylarene [66]. Due to the availability of a well-characterised structure Fe^{IV}=O as well as the Fe^{III}-oxygen species such as Fe^{III}-iodosylarene with 13-TMC (1,4,7,10-tetramethyl-1,4,7,10-tetra aza-cyclotridecane) ligand, makes its comparative study possible. In the study, they have found that the Fe^{IV}=O intermediate was not able to oxidise alkene while if Fe^{III}-iodosylarene introduced with similar reaction conditions, it could perform epoxidation of alkene species. This suggests that Fe^{IV}=O is a sluggish oxidant or does not participate in the oxidation reaction. As the Fe^{V}=O complex with 13-TMC ligand was difficult to synthesise, it has been suggested that the Fe^{V}=O species may be present. But the stereospecific reaction studies neglect the possibility of this species as well.

Very recently, our group published the mechanistic studies on Fe^{III}-iodosylarene in epoxidation reaction of styrene using DFT study [67]. In this study, the electronic structure analysis of Fe^{III}-iodosylarene [(13-TMC)Fe^{III}-OIPh]$^{2+}$ gave the structural and spectral parameters the same as reported in experimental studies. The ground state predicted by the EPR experiment for this complex to be S = 5/2, which was in good agreement with our DFT. Energetic for the direct attack of Fe^{III}-iodosylarene complex to olefin (styrene) to form epoxidation product found to have significantly lower barrier height (53.6 kJ/mol) which corresponds to the simultaneous breaking of I···O bond and O···C bond formation (see Fig. 8a and c). This step released the neutral PhI molecule, which gave the thermodynamic stability for both the products.

On the other hand, the formation of Fe^{IV}=O moiety requires 51.4 kJ/mol energy barrier, which found to be very close to the direct oxygen-atom transfer step. In this case, the olefin attack also requires 32.8 kJ/mol energy to form the epoxide product (see Fig. 8b). One electron transfer pathway from Fe^{IV}=O to PhI$^{\cdot+}$ to form Fe^{V}=O was found to be thermodynamically as well as kinetically unfavourable, and this is consistent with the previous report of Nam and co-workers [65]. The key understanding from this portion is that the formation of high-valent Fe$^{IV/V}$=O depends upon the ligand architecture and depending upon the ligand architecture, the reactivity of the Fe$^{IV/V}$=O species could be higher or lower than their precursor materials.

3. Influence of axial and equatorial ligands on the reactivity of LFe^{IV}=O

Over the last several decades, the high-valent Fe^{IV}=O complexes have made a tremendous contribution to the literature [12,26,68–70]. Various types of ligand frameworks came into the picture to mimic the reactivity of biologically known ones. The biologically

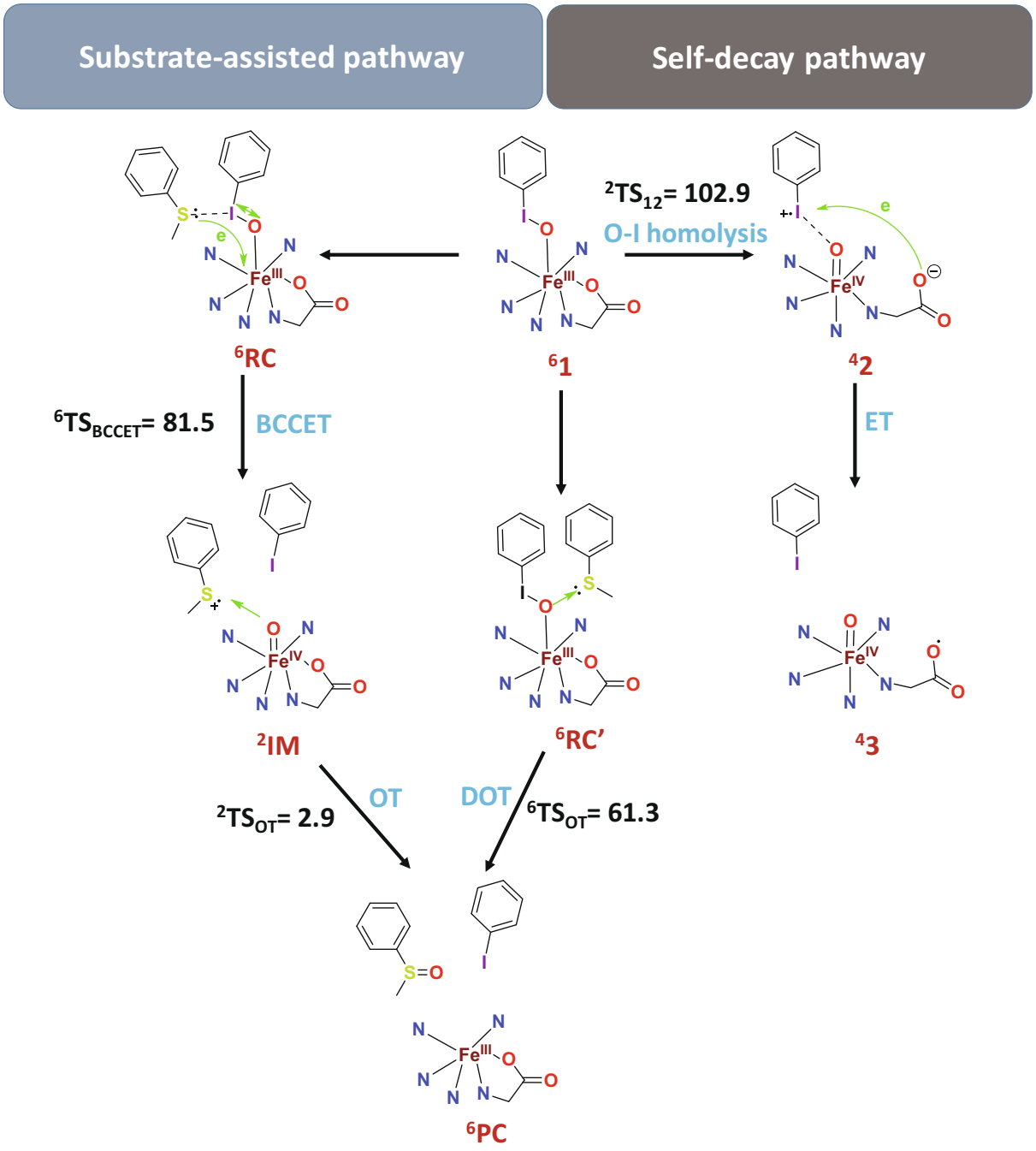

Scheme 5. The mechanistic pathway is redrawn from the Ref. [65]. Here, all the energies are given in the kJ/mol. Superscript shows the ground state multiplicity of the species and transitions states.

known Fe^{IV}=O contains two types of ligand architectures, heme (contains a porphyrin ring) and non-heme (without porphyrin ring). Here, the different kinds of reactions are performed through the specific types of enzymes which differ slightly in their ligand environment. For example, cytochrome P450 (CYP450) heme enzyme Fe^{IV}=O moiety was found to be more reactive when attached to porphyrin radical cation (Cpd I) than that of porphyrin without radical cation (Cpd II) though both contain cysteine at axial position (see Fig. 9) [71–73]. If we look into the ligand environment of Fe^{IV}=O in CYP450 Cpd I (CYP450-I) and horseradish peroxidase Cpd I (HRP-I) (see Fig. 9) [74,75] where both contain radical porphyrin cation but differ in axial ligands cysteine and histidine respectively, former shows "push effect" and later shows "pull effect" on Fe^{IV}=O moiety [76–80]. In push effect, the electron density is donated while in pull effect electron density is withdrawn by the axial ligand to heme Fe^{IV}=O moiety. Due to this, HRP-I unable to react with C–H activating substrate but reacts with hydrogen peroxide to convert it into a water molecule.

These observations attract scientists of this community to deeply understand the nature of binding ligands to Fe^{IV}=O moiety. Here, we divide this part of the review as follows (i) common ligands that stabilise Fe^{IV}=O types of ligands known in the literature (ii) effect of these ligands on reactivity/stability of Fe^{IV}=O moiety.

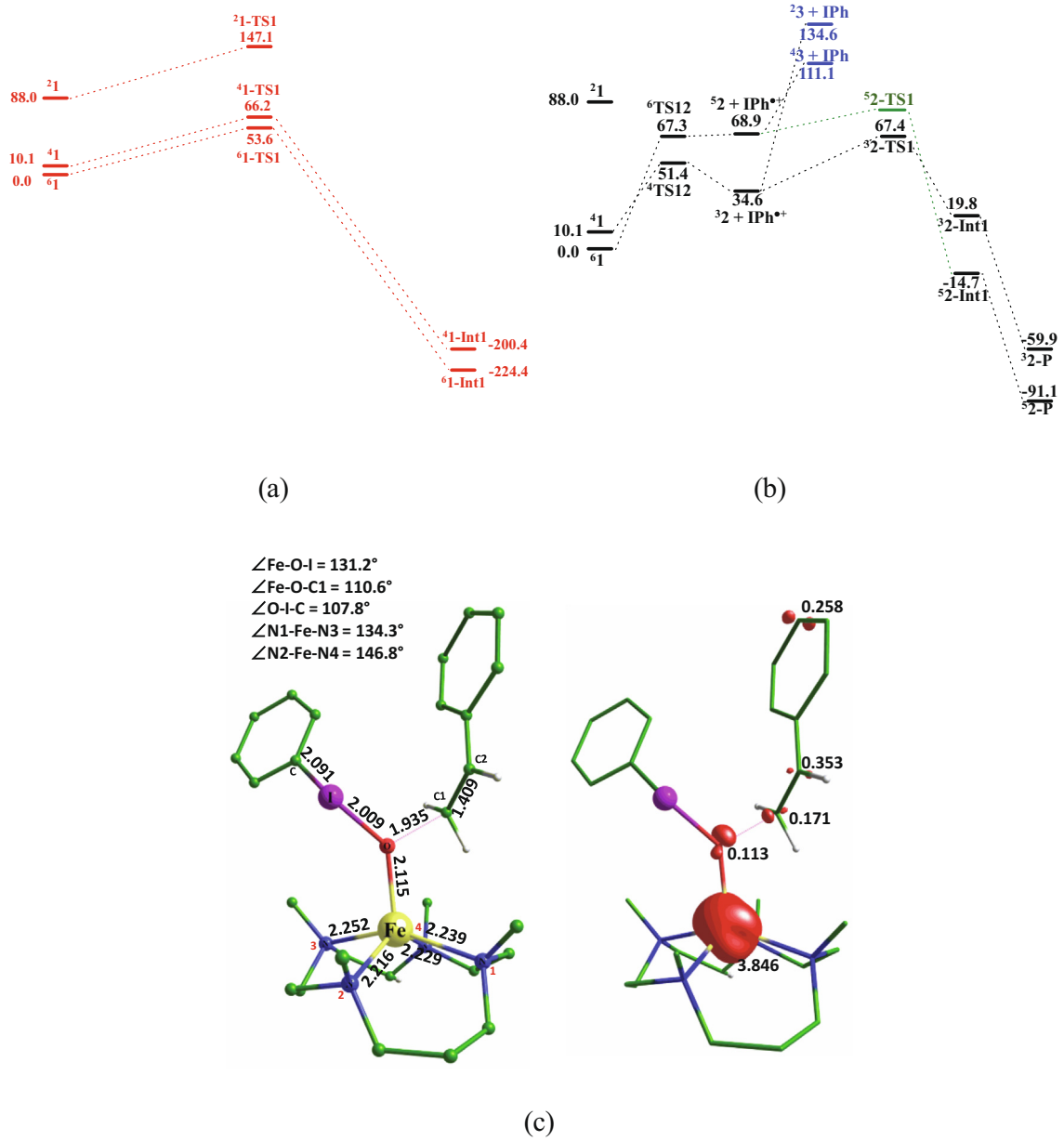

Fig. 8. Energy profile computed for (a) direct epoxidation pathway, (b) epoxidation through formation $Fe^{IV/V}$=O and (c) optimised geometry and spin density of lowest transition state of direct epoxidation. Reprinted (Adapted) with permission from Ref. [67]. Copyright (2019) Indian Chemical Society.

(i) Common Ligands that stabilise Fe^{IV}=O moiety

In the high-valent iron chemistry, many types of ligand architectures are known in the literature. Here, we limit our discussion to ligand architecture where axial and/or equatorial ligand effects are probed. The first classical ligand framework in the Fe^{IV}=O chemistry is porphyrin radical cation ($Por^{\bullet+}$) which has four nitrogen donor groups. It can occupy four coordination sides in the equatorial plane of Fe^{IV}=O moiety due to their rigid geometry. This was the first example from biology, where porphyrin equatorial ligand modification and axial ligand effects have been tested rigorously [9,10,71,81–83]. The synthesis and characterisation of first iron(IV)-oxo based on $Por^{\bullet+}$ came into the picture in 1981 [81]. As time passes, new types of ligands are developed to study the nature of Fe^{IV}=O moiety. In the literature, most of the reported ligands contain nitrogen donor atoms. These atoms have the moderate σ-donating ability towards Fe^{IV}=O moiety compared to oxygen (low σ-donating ability) and carbon (high σ-donating ability).

The main criteria for a look into the new types of ligand architecture are to mimic the reactivity of enzymes/enhance the reactivity of Fe^{IV}=O moiety. In the non-heme framework, one of the thoroughly studied ligands belongs to the so-called TMC (TMC = Tetramethylcyclam) ligand where X-ray structure of Fe^{IV}=O was solved [84], triggering great interest in this chemistry (see Scheme 6 for various ligands reported) [63]. After the discovery of these ligand frameworks, iron(IV)-oxo with aminopyridine-based ligand frameworks such as N-benzyl-N,N′,N′-tris(2-pyridylmethyl)ethylene-diamine (BnTPEN) [85], tri(2-pyridylmethyl)amine (TPA) [86], N,N-bis(2-pyridylmethyl) bis(2-pyridyl)methylamine (N4Py) [87] etc. (Scheme 6) came into the picture and latest N-heterocyclic carbene based ligand 3,9,14,20-tetraaza-1,6,12,17-tetraazoniapenta-cyclohexacosane 1(23),4,6(26),10,12(25),15,17(24),21-octaene) (L^{NHC}) [88] (Scheme 6) was developed and studied for equatorial ligand effect.

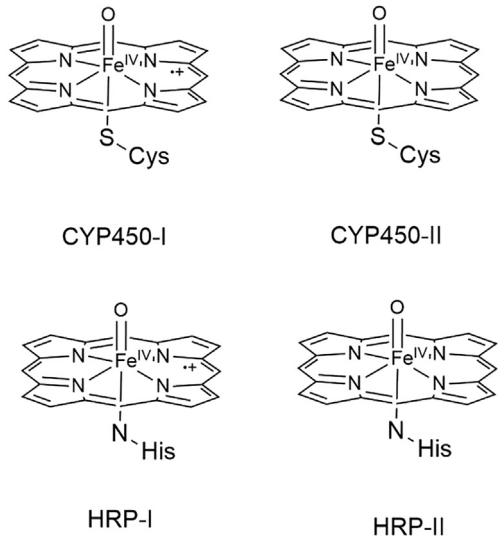

Fig. 9. Representative structures of cytochrome P450 (CYP450) and horseradish peroxidase (HRP) compound I and compound II.

(ii) Effect of ligands on Fe^{IV}=O

Axial ligand effects around Fe^{IV}=O moiety are thoroughly discussed and reviewed in the literature [26,45,68,82,89–96], and therefore here we focus on the effect of equatorial ligands. We will start our discussion from a model system study performed by Li and co-workers [97]. They have studied the Fe^{IV}=O catalysed C–H activation of methane for complexes in which five negatively charged (CN^-, NC^-, F^-) ligands are surrounded. Here, they have analysed the reaction pathways (σ-pathway and π-pathway) in the simple $[(CN)_5Fe^{IV}=O]^{3-}$ model and then gradually substituted the CN^- ligands with NC^- or F^- ligands. Neese and co-workers [98] define the four possible pathways; two each for S = 1 and S = 2 spin states (see Fig. 10). The α-electron of C–H bond is transferred to $\sigma^*d_z^2$ orbital and this leads to the σ-pathway while β-electron transfer to gives a $\pi^*_{xz/yz}$-pathway. The Fe-O–H angle during H-transfer should lie ~180° and ~120° in σ- and π-pathways, respectively. Classically followed pathways for S = 2 and S = 1 are σ and π, respectively. Generally, the σ-pathway is found to be lower in energy compared to π-pathway with Fe-O–H angle nearly 180°. But model systems studied reveal a new hybrid σ + π pathway with a Fe-O–H angle around 120° is observed for the quintet state. After discussing the relatively simpler equatorial ligands now, we will turn to discuss some larger equatorial ligands. Past studies suggest that the redox potential of Fe^{IV}=O complexes has a profound role in the nature of equatorial ligands [99,100]. The experimental studies using various types of equatorial ligands affect the redox potential. If a strong equatorial ligand is attached to the Fe^{IV}=O moiety, this would destabilise the d_{x2-y2} orbital relative to the d_{xy} orbital leading to the lower HAT rate. This observation was seen by the blue shift of the near-IR spectral feature of Fe^{IV}=O moiety. This will lead to the higher triplet and quintet spin state gap, which reduces the mixing of S = 2 spin state.

Recently, Meyer's group synthesise and characterized a N-heterocyclic carbene (NHC) based Fe^{IV}=O complexes $[(L^{NHC})Fe^{IV}=O(CH_3CN)]^{2+}$ species (L^{NHC} = 3,9,14,20-tetraaza-1,6,12,17-tetraazo niapenta-cyclohexane cosane-1(23),4,6(26),10,12 (25),15,17 (24),21-octaene) [88]. A thorough spectroscopic study on this complex in comparison to the N-coordinated $[(SR\text{-}TPA)Fe^{IV}=O(CH_3CN)]^{2+}$ (SR-TPA = tris(3,5-Dimethyl-4-methoxypyridyl-2-methyl) amine) using experiment and theory have been performed by the same group in collaboration with Neese group [101]. The NHC ligand structure was very similar to the porphyrin moiety. To understand the equatorial ligand effect on the Fe^{IV}=O moiety, this was the ideal geometry in case of larger systems. DFT studies on this complex revealed that strong σ-donation through the tetracarbene leads to destabilisation of d_{x2-y2} orbital compared to d_{z2} orbital (see Fig. 11). Variation in the electronic structure leads to our curiosity to study the reactivity of this complex compared to the regularly known porphyrin-based complex CYP 450 Cpd-II $[(Por)Fe^{IV}=O(SH)]^-$ towards the C–H activation [46]. Simultaneously, the reactivity studies in comparison with various substrates along with known Fe^{IV}=O complex have been performed using DFT [102] as well as ab-initio methods [103]. Here, they found that the energy difference between the quintet and triplet spin state of tetracarbene complex (93.1 kJ/mol) was almost three times larger (38.7 kJ/mol) than porphyrin-based complex.

The reactivity studies revealed that the reaction exclusively proceeds through triplet spin surface while quintet surface lies higher in energy for HAT reaction. In this study, both the classical ($^5\boldsymbol{\sigma}$, $^3\boldsymbol{\pi}$) and non-classical ($^3\boldsymbol{\sigma}$, $^5\boldsymbol{\pi}$) reaction channels were explored (see Fig. 10). The involvement of non-classical channels during the C–H bond activation suggested for small systems previously were ruled out [97] whereby the reaction proceeds through lower-lying $^3\boldsymbol{\pi}$ channel for HAT reaction. Previous studies suggested that this channel lies higher in energy for regular N-donor ligand as well as the porphyrin P450 Cpd-II complex.

Theoretical studies reported previously gives a linear relationship between the BDE and barrier height, as mentioned earlier [78,104–107]. If axial or equatorial ligand changes the bond dissociation energy of metal-OH bond, this will also alter the barrier height i.e., higher BDEs are associated with lower barrier height and vice-versa. As mention previously, BDEs are related to two fundamental thermodynamic properties such as electron affinity (EA) and basicity ferryl-oxygen which are inversely related. These two factors found to alter by the variation in the axial/equatorial ligands offering a convenient way to fine-tune the reactivity. Further on, the hydroxylation of alkane by the heme oxygenases [104,105,108,109] found to be strongly correlated to these two factors mentioned.

In our study, we have attempted to understand the effect of the axial ligand when a strong σ-donating equatorial ligand is present. Here, we have tested various axial ligands such as CH_3CN, SH^-, $N(CH_3)_3$ and $P(CH_3)_3$ as shown in Scheme 7 and found that the axial ligands are not significantly influencing the reactivity of Fe^{IV}=O complexes. Our results wherein the negligible effect of the axial ligand when a strong σ-donating equatorial ligand is coordinated is consistent with the earlier reports [97].

Another, important contribution where the role of equatorial pyridine donation in stabilizing the quintet state and hence enhancing the reactivity by comparing five different non-heme Fe^{IV}=O species have been reported by Wang et al. in 2013 using extensive spectral, analytical and reactivity studies [110]. Their study concludes that when the pyridine ligands are perpendicular to the Fe=O bond, its reactivity is larger compared to ligand architecture when they are parallel.

In continuation of the discussion, recent reports [111–113] with small perturbations on the equatorial ligands have been notified. The addition of methyl groups on the pyridine ring of N4Py ligand or replacing two of the pyridine with quinoline/benzimidazole such as given below in Fig. 12, leads to fine-tuning the reactivity due to electronic and steric factors. Here, secondary-coordination play an important role in altering the reactivity of the given complexes. These interactions affect π^*_{xy} and σ^{*2}_{xy} orbitals, N_{ax}-Fe=O angle, and approach of the substrate with the oxidant which eventually decreases the triplet and quintet gap and increases the reactivity of these complexes compared to unperturbed complex. Que and Visser's group have performed studies using 2pyN2Q/2pyN2B ligands and the reactivity order was found to be $[(N4py)Fe^{IV}=O]^{2+}$< $[(2pyN2B)Fe^{IV}=O]^{2+}$< $[(2pyN2Q)Fe^{IV}=O]^{2+}$ [111,113] and this found

Heme Ligands

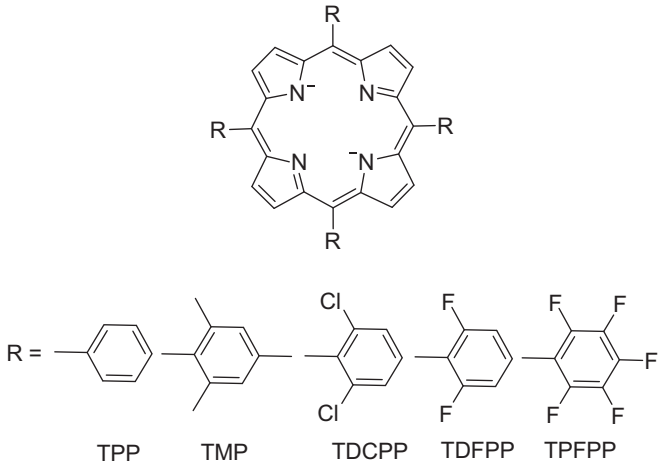

Nonheme Ligands

TMC-based Ligands

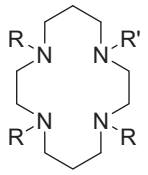

Me_3cy-py: R=Me, R'=CH_2Py
Me_4cy: R=R'=Me
cy: R=R'=H
cy-ac: R=H, R'=CH_2COO-
Me_3cy-ac: R=Me, R'=CH_2COO-
Me_3cyS: R=Me, R'=CH_2CH2S-

Aminopyridine-based Ligands

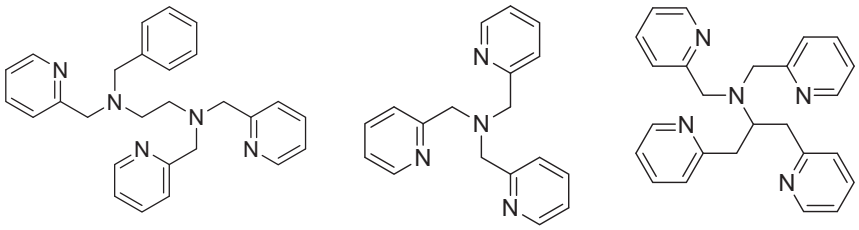

Carbene-based Ligands

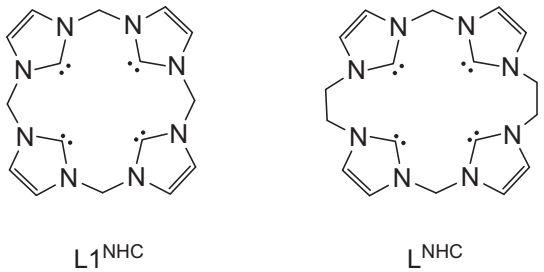

Scheme 6. Synthetic ligand structures present in the literature.

to correlate well with the triplet-quintet energy gap computed. Further, Visser and co-workers have reported that the triplet-quintet gap decreases from 17.6 kJ/mol (N4Py), to 16.8 kJ/mol reported for (^{Me,Me}N4Py) and 9.7 kJ/mol ($_{Me,Me}$N4Py) which is also in line with the highest reactivity of ^{Me,Me}N4Py among these complexes [112]. Absolute value of the triplet-quintet energies are not comparable

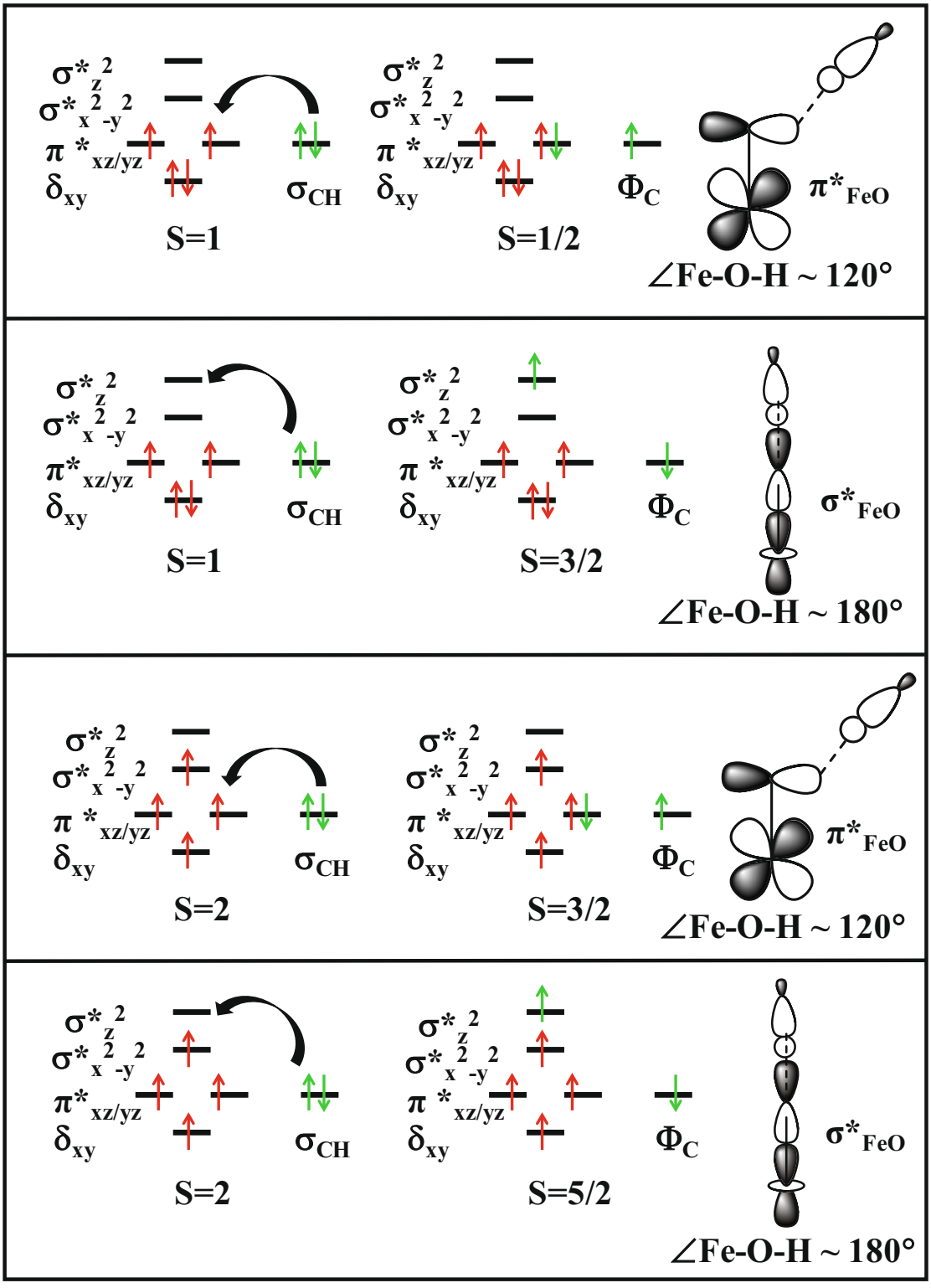

Fig. 10. Possible σ- and π-pathways for S = 1 and S = 2 spin state.

among different ligands (due to variation in functional/basis set used)and therefore it is wise to compare the difference of difference between the triplet-quintet gap i.e [$E_{T\text{-}Q}$(2pyN2Q/ ^{Me,Me}N4Py)-$E_{T\text{-}Q}$(N4Py)] and this analysis reveal that this gap is 7.9 kJ/mol for $_{Me,Me}$-N4Py and 19.7 kJ/mol for 2pyN2Q both with respect to N4Py, reflecting higher reactivity for the later species.

4. Reactivity of $Fe^{V/IV}$=O towards selective halogenation

The formation of carbon-halogen bond in many natural products is synthetically very much important due to their substantial therapeutic significance, e.g., vancomycin, chlortetracycline, chloramphenicol, etc. [114,115]. A group of enzymes that consist of

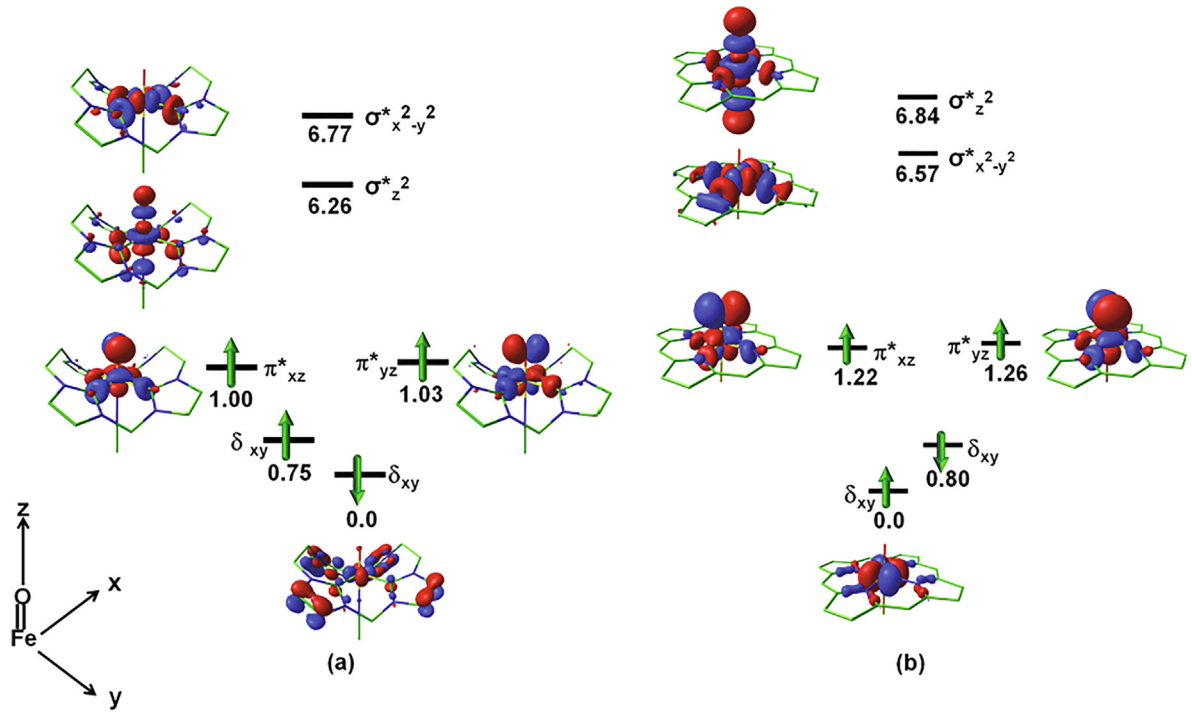

Fig. 11. Orbital swapping diagram. Reprinted (Adapted) with permission from [46]. Copyright (2018) Wiley-VCHVerlag GmbH.

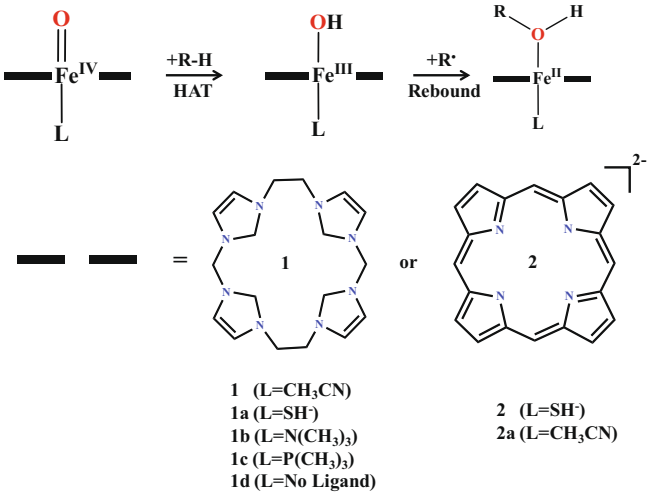

Scheme 7. The hydroxylation process by tetracarbene and cytochrome P450 Cpd-II Fe^{IV}=O reagents with variable axial ligands: **1** ($[(L^{NHC})Fe^{IV}=O(CH_3CN)]^{2+}$), **1a** ($[(L^{NHC})Fe^{IV}=O(SH)]^{+}$), **1b** ($[(L^{NHC})Fe^{IV}=O(N(CH_3)_3)]^{2+}$), **1c** ($[(L^{NHC})Fe^{IV}=O(N(CH_3)_3)]^{2+}$), **2** ($[(Por)Fe^{IV}=O(SH)]^{-}$) and **2a** ($[(Por)Fe^{IV}=O(CH_3CN)]$). Reprinted (Adapted) with permission from Ref. [46]. Copyright (2018) Wiley-VCHVerlag GmbH.

Fe(II), α-ketoglutarate (αKG), O_2 and halogen ligands in their active site govern the incorporation of the halogen atom in the unactivated aliphatic compounds. The SyrB2 [32] is one of the halogenase which performs chlorination of the γ-carbon of L-Thr. Similarly, CytC3 [33,34] catalyse the chlorination of γ-methyl group of L-2-aminobutyric acid [34], and another halogenase CmaB catalyses the biosynthesis of the one-step of coronatine, a leaf protein [116]. Therefore, interest has been drawn from various research groups to study the mechanistic pathways of these halogenase metalloenzymes. It was proposed that the key reactive intermediate in halogenases is a high-spin oxo-ferryl species [35].

It is experimentally observed that, in these halogenases, a halogen (Cl/Br) ligand is attached to the Fe-center in the active site, which is normally occupied by a carboxyl group in oxygenases. The key steps involved first, the formation of an X-Fe^{IV}=O intermediate followed by hydrogen atom abstraction from substrate catalysed by the Fe^{IV}=O species [25,117,118]. In the preceding step, the halogen atom is transferred to the radical substrate in a rebound mechanism forming a halogenated product (see Scheme 8). Fujimori et al. [33] had studied the chlorination reaction of L-Aba-S-CytC2 (Aba = aminobutyrate) catalysed by halogenase CytC3 from *Streptomyces* [34] and observed a mixture of two positional isomers of high-spin Fe^{IV} complexes remains (Oxo trans to axial histidine vs. cis to axial histidine) in equilibrium after C–H bond cleavage.

Over the decades, several computational studies have been performed to elucidate the mystery behind exclusive chlorination by halogenase, SyrB2. Later Siegbahn group has performed a theoretical calculation on a small model containing all first coordination spheres and several second coordination sphere ligands (see Fig. 13) around Fe^{IV}=O centre of this metalloenzyme to clarify the ambiguous nature of the selective chlorination over hydroxylation [35]. A truncated L-Thr, loaded on the phosphopantetheine arm was taken as substrate. It is seen that in native SyrB2 the ligand bound to the transposition of His235 is preferentially transferred to the carbon radical resulting selective halogenation.

DFT calculations on both of the positional isomeric Fe^{IV}=O species, which are confirmed via Mossbauer spectra, indicates that stabilisation via hydrogen bonding interaction with the neighbouring water molecules plays an important role in deciding the barrier for the hydrogen abstraction step leading to the formation Fe^{III}-OH/cyclohexyl radical system as well as dictates the stability of the Fe^{III}-OH/cyclohexyl radical intermediate. In one isomer where the oxo ligand is in trans to the axial His-235, hydroxylation reaction is favoured whereas, in the stereoisomer where the chloro group changes its position with the oxo group and secured transposition of the His235, chlorination occurs preferentially (see Scheme 9). This concluded that the arrangement which makes the chloride

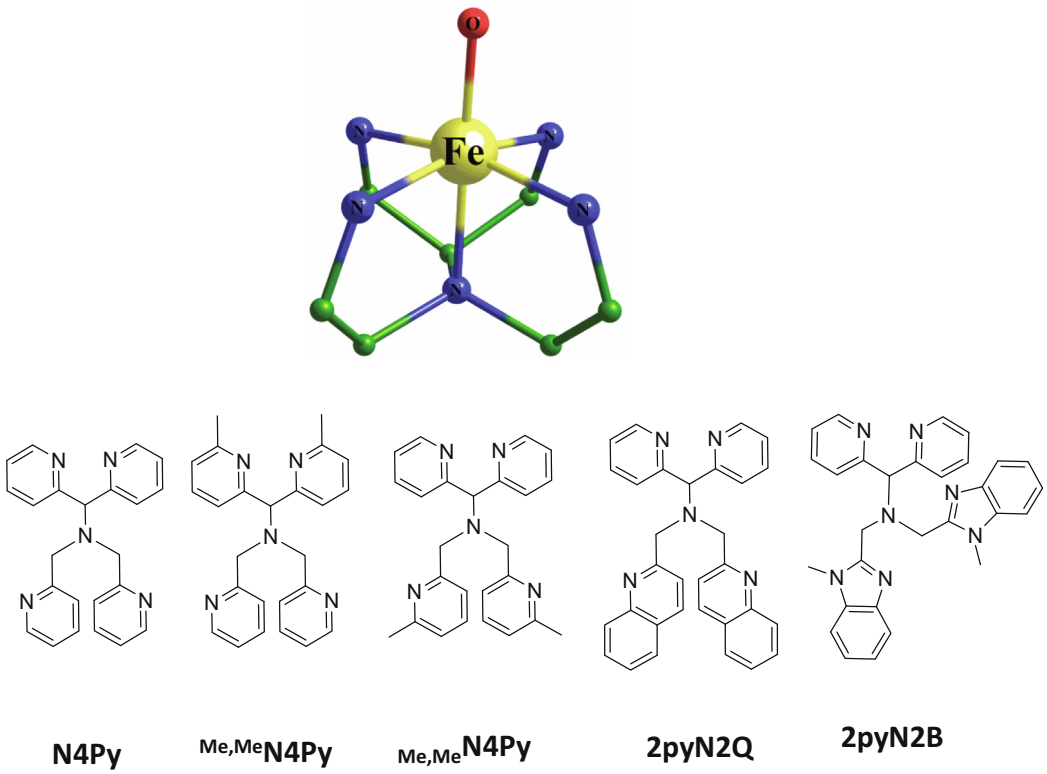

Fig. 12. Small equatorial ligand perturbations around the fixed tertiary amine moiety in the octahedral environment.

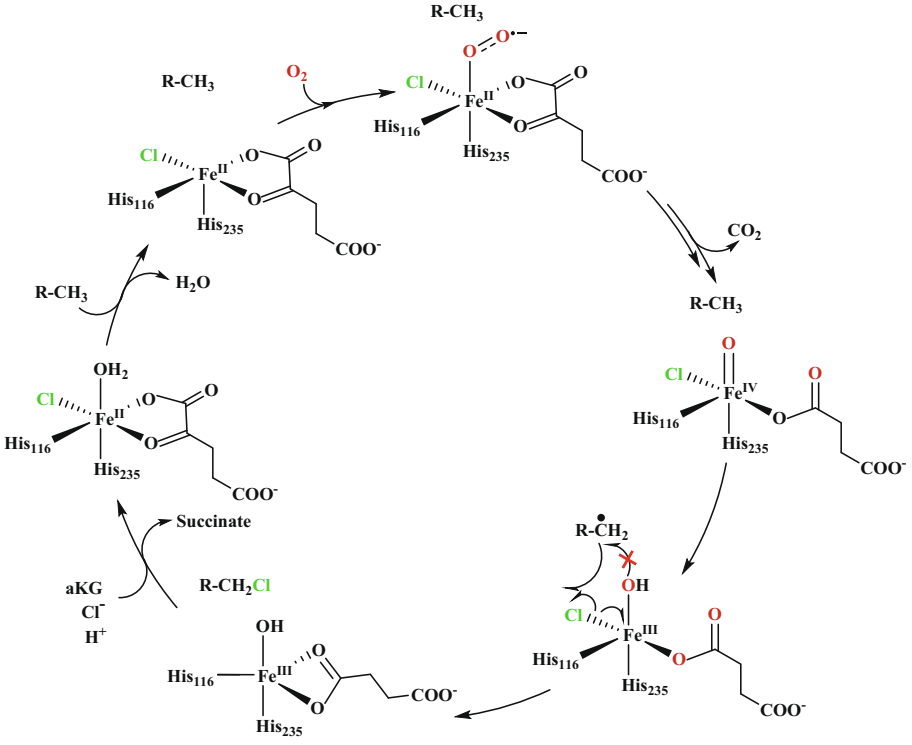

Scheme 8. General mechanism of the halogenation catalyzed by naturally occurring SyrB2 halogenase. Reprinted (Adapted) with permission from Ref. [35]. Copyright (2010) American Chemical Society.

ligand closer to the carbon radical than that of the –OH ligand (see Fig. 14) will give selective halogenation. The important bonding parameters and the energies of the ground state, as well as the lowest energy transition states, are tabulated in Table 1.

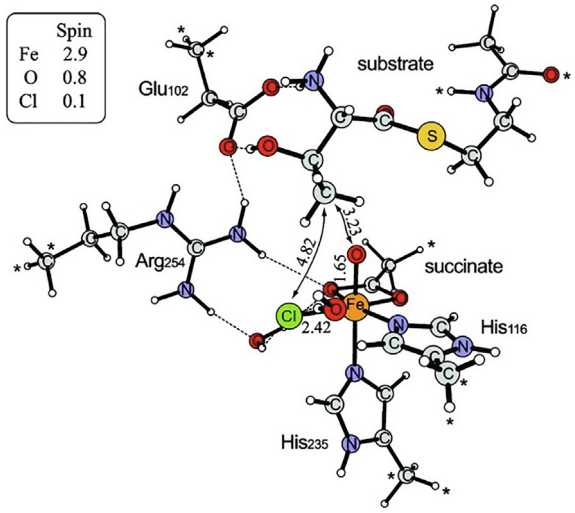

Fig. 13. Active site model structure for the DFT calculation. Atoms marked as asterisks kept as fix during the optimization. Reprinted (Adapted) with permission from Ref. [35]. Copyright (2010) American Chemical Society.

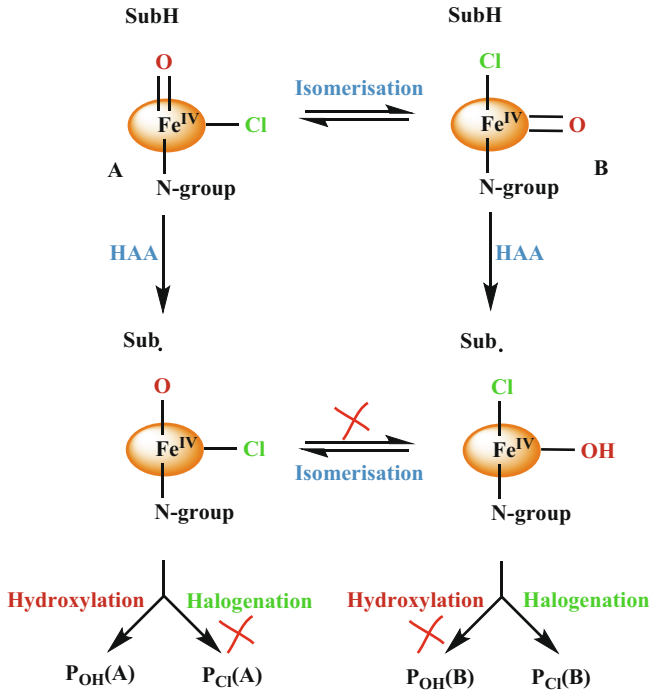

Scheme 9. Schematic representation of the halogenation vs. hydroxylation of L-thr with the biomimetic model of SyrB2 enzyme.

In this direction, Burton and co-workers have introduced a small active site cluster model (M1, Fig. 15) of halogenase SyrB2 metalloenzyme containing the Fe^{IV}=O moiety, two histidine molecules (truncated through the C–C bond), α-KG group, the chloride ligand and ethane as a substrate [119]. This model is failed and is ending up with selective hydroxylation over chlorination. After the failure of the model M1, DFT calculation with a second model M2, which is exactly similar to model M1 except for a protonated Arg254, modelled as ethyl guanidium, placed near the active site results in increasing the hydroxylation barrier while lowering the barrier of chlorination (see Table 1) though with a small difference in barrier of 13.4 kJ/mol. Here arginine is getting involved in the hydrogen bonding with the Fe-OH group (reflected by the short hydrogen-bond length between Arg254 and the Fe-OH group) making the OH group less available for the hydroxylation. In this work, they have anticipated that to achieve the selectivity for the specific iron-bound OH or Cl ligand; the substrate molecule needs to be in close proximity.

Another mechanism with model M1 was predicted which is leading to selective chlorination exclusively where the OH group for the rebound reaction becomes inaccessible due to protonation and ending up giving coordinated water molecule. They have identified the Glu102 residue (present in the protein crystal structure hydrogen-bonded to the Arg254 residue) as a protonation source of the Fe-OH group in a shuttle mechanism. Therefore, it can be proposed that to mimic the selectivity of the native halogenase, it is the nearby amino acid residues which are responsible for the enhancement of the rate of the chlorination and suppression of the rate of hydroxylation

A similar study of Visser and co-workers on a biomimetic model complex of TauD, containing Fe^{IV}=O system which is coordinated to two imidazole groups (mimic of two histidine groups), α-ketopropionate (mimic of α-ketoglutarate), a chloride ion, propene as substrate molecule and carbon dioxide [36]. After DFT calculations on this model system, they have shown a low energy pathway where the carbon dioxide byproduct from an earlier step in the catalytic cycle attacks the hydroxyl group in the Fe^{III}-OH moiety leading to the formation of bicarbonate complex and halogenated product (see Scheme 10). This low-energy alternative path leads to the formation of the chlorinated product by pushing away the hydroxyl group from the reaction centre, hindering it from attack to the allyl radical, and prevent hydroxylation. In this study, it is shown that in hydroxylases, this type of –OH group trapping is not favoured. In the TauD model system, the –OH group trapping barrier is raised due to the repulsive interaction between the CO_2 molecule and the negatively charged OH group. This mechanism is in line with the experimental observations and gave a suitable explanation for the halogenation over hydroxylation.

Siegbahn and co-workers have reported first biomimic non-heme iron(III)-halide complex $[(TPA)(Cl_2)Fe^{III}]^+$ to employ halogenation to sp^3 C–H bond. In this study, X–Fe^V=O, $[(TPA)(Cl)Fe^V=O]^{2+}$ was depicted as the active intermediate towards halogenation (see Fig. 16) [120]. The formation of the $[(TPA)(Cl)Fe^V=O]^{2+}$complex from $[(TPA)(Cl_2)Fe^{III}]^+$ species and the probable reaction mechanism of the halogenation of cyclohexane is depicted in Scheme 11. The low energy isomer $[(TPA)(Cl)Fe^V=O]^{2+}$ N_{amine} complex (see Fig. 16), being a very strong oxidizing agent (gas-phase electron affinity = −1032.4 kJ/mol and ionization potential of cyclohexane in gas-phase = 938.3 kJ/mol), can oxidize cyclohexane before any bond formation. This results in a cyclohexyl cation and reduction of the charge of the Fe-catalyst from +2 to +1. The DFT calculations on this system indicate a concerted reaction mechanism where for both possible spin states, M = 4_{is} and M = 4_{hs}, there is a direct hydrogen atom abstraction from the substrate without the formation of any intermediate leading to the chlorinated product in a concerted manner.

In the cyclohexyl-$[(TPA)(Cl)Fe^{IV}=O]^+$ species, the substrate cation is pointing towards the chloride ligand, and hydroxide group stays away from the substrate due to the repulsion between the positively charged substrate and the $[(TPA)(Cl)Fe^{IV}=O]^+$ species eliminating the possibility for the hydroxylation. At the time of hydrogen abstraction, the substrate is bent between the oxo and the chloride group, Fe-Cl bond is being elongated, and the substrate is attracted towards chloride resulting in immediate bond formation (see Fig. 17). Therefore, it can be concluded that the exclusive chlorination immediately after hydrogen atom abstraction is guided by the proper orientation of the substrate molecule in a beneficial way.

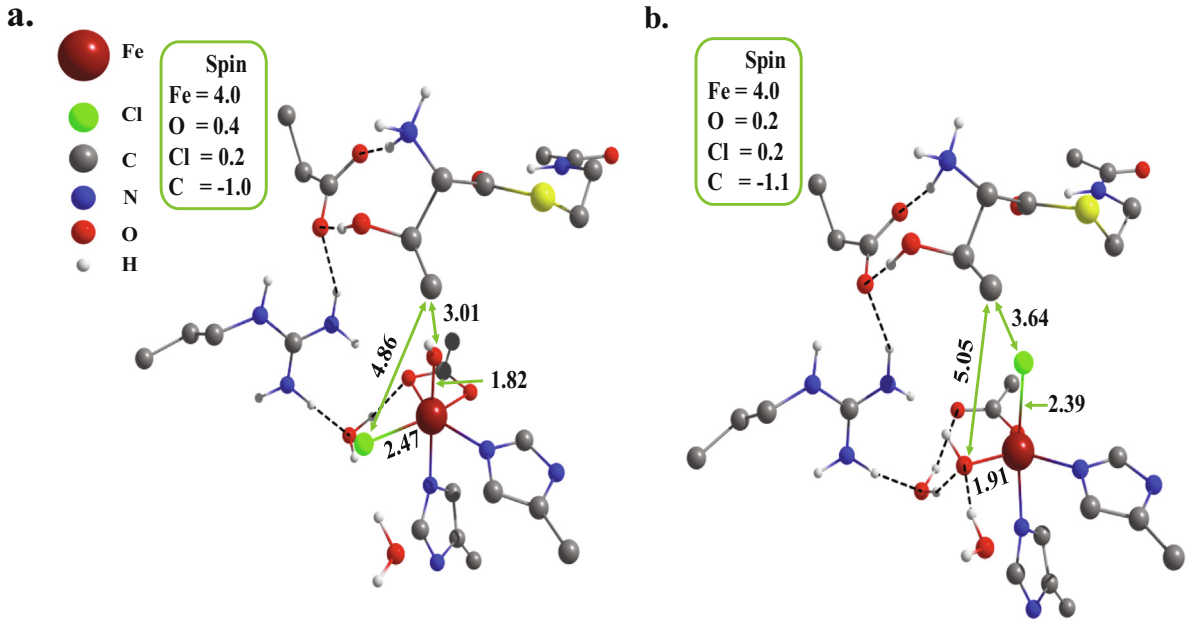

Fig. 14. Optimized structures for (a) Fe^{III} –OH intermediate b, (b) Fe^{III}-OH intermediate b′. Reprinted (adapted) with permission from Ref. [35]. Copyright (2010) American Chemical Society.

Table 1
Important feature of the various Fe^{IV}=O catalyst that is reported to perform halogenation vs. hydroxylation processes.

Species	Ground State Spin (GS)	Fe-O/N (GS, Å)	HAA-Barrier Height (kJ/mol)	Fe-O/N (TS, Å)	Reactivity Pattern (S*)	Hydroxylation/Halogenation Barrier Height (kJ/mol)	Substrate	Ref.
L1Fe^{IV}=O (isomer *a*)	S = 2	1.650	77.3	1.760	S = 2	34.4/72.7	Truncated L-Thr	[35]
L1Fe^{IV}=O (isomer*a*′).	S = 2	1.670	74.3	1.870	S = 2	36.5/22.3	Truncated L-Thr	[35]
L2Fe^{IV}=O(model M1)	S = 2	1.610	53.8	1.730	S = 2	19.7/26.0	Ethane	[119]
L3Fe^{IV} = O(model M2)	S = 2	–	–	–	–	29.4/15.9	Ethane	[119]
L4Fe^{IV}=O	S = 2	1.652	29.4		S = 3	27.7/44.1 27.7/7.1 (alternative path)	Propene	[36]
[(TPA)(Cl)Fe^{V}=O]$^{2+}$	S = 1	1.680	39.9	–	S = 2	14.2/21.2 (in S = 5) 26.8/21.4 (in S = 3)	Cyclohexane	[120]
L5X-Fe^{IV}=O	S = 2	1.640	51.9	–	S = 2	Very less selectivity	Cyclohexane	[38]
[(2PyN2Q)Fe^{IV}=O)]$^{2+}$	S = 1	1.626	69.4	1.693	S = 2	173.04/51.3	Cyclohexane	[41]

L1 = two histidine ligands, one chloride, α-kG group in the first coordination sphere along with Arg254, Glu102 and two water molecules in the second coordination sphere.
L2 = two histidine molecules (truncated through the C–C bond), α-KG group, chloride ligand.
L3 = two histidine molecules (truncated through the C–C bond), α-KG group, the chloride ligand, and ethane as a substrate and Arg254 modelled as ethyl guanidinium.
L4 = two imidazole groups (mimic of two histidine groups), α-ketopropionate (mimic of α-ketoglutarate), a chloride ion and carbon dioxide.
L5 = 3,7-dimethyl-9-oxo-2,4-bis(2-pyridyl)-3,7-diazabicyclo[3.3.1]nonane-1,5-dicarboxylate methyl ester.
S*= lowest energy transition spin state.

Finally, we can conclude here that, the substrate orientation is very important to get the selectivity and it can be a guide to the experimentalists to achieve the exclusive chlorination by the appropriate ligand designing which can give a proper arrangement of the substrate towards the halide moiety.

Later, Visser and co-workers studied the reactivity of [(TPA)(Cl)Fe^{IV}=O]$^{+}$ (see Fig. 18) with ethylbenzene as a substrate [37] to find the answer on whether this type of isomerization is possible in biomimetic nonheme Fe^{IV}=O species and can be achieve the regioselectivity in a similar manner. The calculations have revealed that when the oxo ligand is trans to the amine group of TPA ligand, hydroxylation is favoured whereas when the oxo group is in the *cis* position, the reaction is ended up with the chlorinated product. Experimental studies using the concerned catalyst [(TPA)(Cl)Fe^{IV}=O]$^{+}$ suggested giving the only halogenated product. To find the reason behind the removal of the cis ligand in the rebinding phase, they have performed thermodynamic studies. The calculation has shown that there is a change in Fe-Cl and Fe-OH bond strength between the two isomers by which a weaker ligand occupies the *cis* position.

The exclusive production of a halogenated product by the naturally occurring halogenases depends on the following factors, 1) hydrogen bonding arrangements at the active site, 2) positioning of the substrate, 3) redox potentials of the rebound sites that are reported to have the order Br < Cl < OH 4) last but not the least factor is unavailability of OH site via the formation of bicarbonate or by protonation of the hydroxyl group.

Later on Comba et al. has proposed a non-heme iron-bispidine complex, [Fe^{II}(L)Cl_2] (L = 3,7-dimethyl-9-oxo-2,4-bis(2-pyridyl)-3,7-diazabicyclo[3.3.1]nonane-1,5-dicarboxylate methyl ester), with hydrogen peroxide (H_2O_2), tertiary butyl hydroperoxide (TBHP) or iodosylbenzene (PhIO) as external oxidant, which effectively oxidize and halogenate cyclohexane [38]. It is the first report on the functional halogenase model. It is shown that the product selectivity and the preferred pathway is extensively dependent on the oxidizing agent used during the reaction. Quantum mechanical

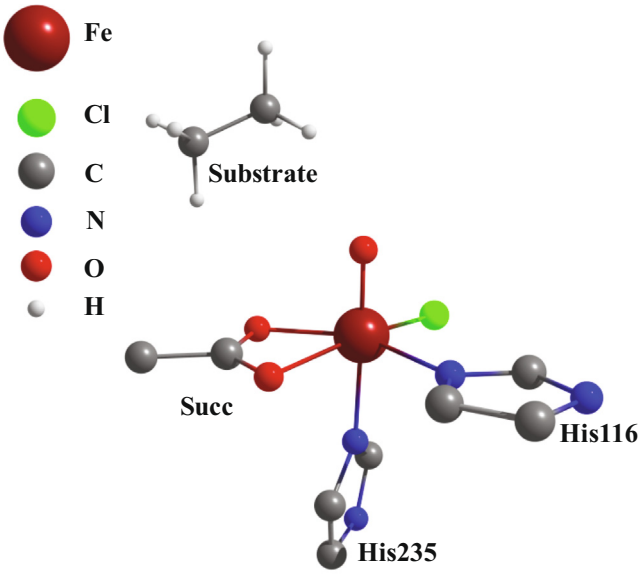

Fig. 15. Model M1, reactant structure (Fe^{IV}=O system with the ligand in the first coordination sphere. Reprinted (adapted) with permission from Ref. [119]. Copyright (2009) Royal Society of Chemistry.

calculations were implemented to explore the catalytic reaction mechanism governed by the two probable reaction channels of X-Fe^{IV}=O and X-Fe^{V} = O (X = Cl, Br) as reactive intermediates. Calculations reveal that S = 2 high spin state is found to be the ground state which is consistent with previously reported non-heme halogenases [38]. DFT study reveals that, although the formation of $[(bispidine)(Cl)Fe^{V}=O]^{2+}$ complex via heterolytic cleavage of the O-O bond of the Fe^{III}-OOH precursor, is less favourable than its Fe^{IV}=O isomer, once it forms the halogenation process is barrierless. In this case, hydrogen abstraction is found to be barrierless, and the lone pair of the coordinated halide pointed towards the singly occupied molecular orbital of the cyclohexyl radical leading the potential energy surface to the direct halogenation of alkane.

All the above-described reactions reveal that it yields a mixture of products, i.e., till now, exclusive halogenation is proved to be very difficult. In this direction, Que and co-workers in 2016 has reported a S = 2 Fe^{IV}=O complex $[(TQA)(CH_3CN)Fe^{IV}=O]^{2+}$ (TQA = tris-(quinolyl-2-methyl)amine) [39]. This is a biomimetic model of Fe^{IV}=O intermediate species of non-heme iron enzyme taurine dioxygenase which effectively gives a hydroxylated product. After addition of one equivalent of NBu_4X (X = Cl or Br) to $[(TQA)(CH_3CN)Fe^{IV}=O]^{2+}$ at −40 °C ligand exchange happens resulting in the formation of Fe^{IV}=O complexes $[(TQA)(Cl)Fe^{IV}=O]^{+}$ and $[(TQA)(Br)Fe^{IV}=O]^{+}$ in MeCN as solvent. DFT calculation on the halogen inserted structures (see Fig. 19) has been estimated, and Fe-O bond is found to be 1.64 Å, which is in good agreement with the previously reported values and Fe-Cl and Fe-Br distance is calculated to be 2.36 and 2.51 Å.

With the $[(TQA)(Cl)Fe^{IV}=O]^{+}$ and $[(TQA)(Br)Fe^{IV}=O]^{+}$ complexes in the identical reaction condition, the yield for the halogenated products is 3–6 times higher than that of the oxygenated products. This is the first example of a biomimetic model of halogenases SyrB2 and CytC3. In this study, the author has explained that the X-Fe^{IV}=O species is responsible for the C–H bond cleavage in the

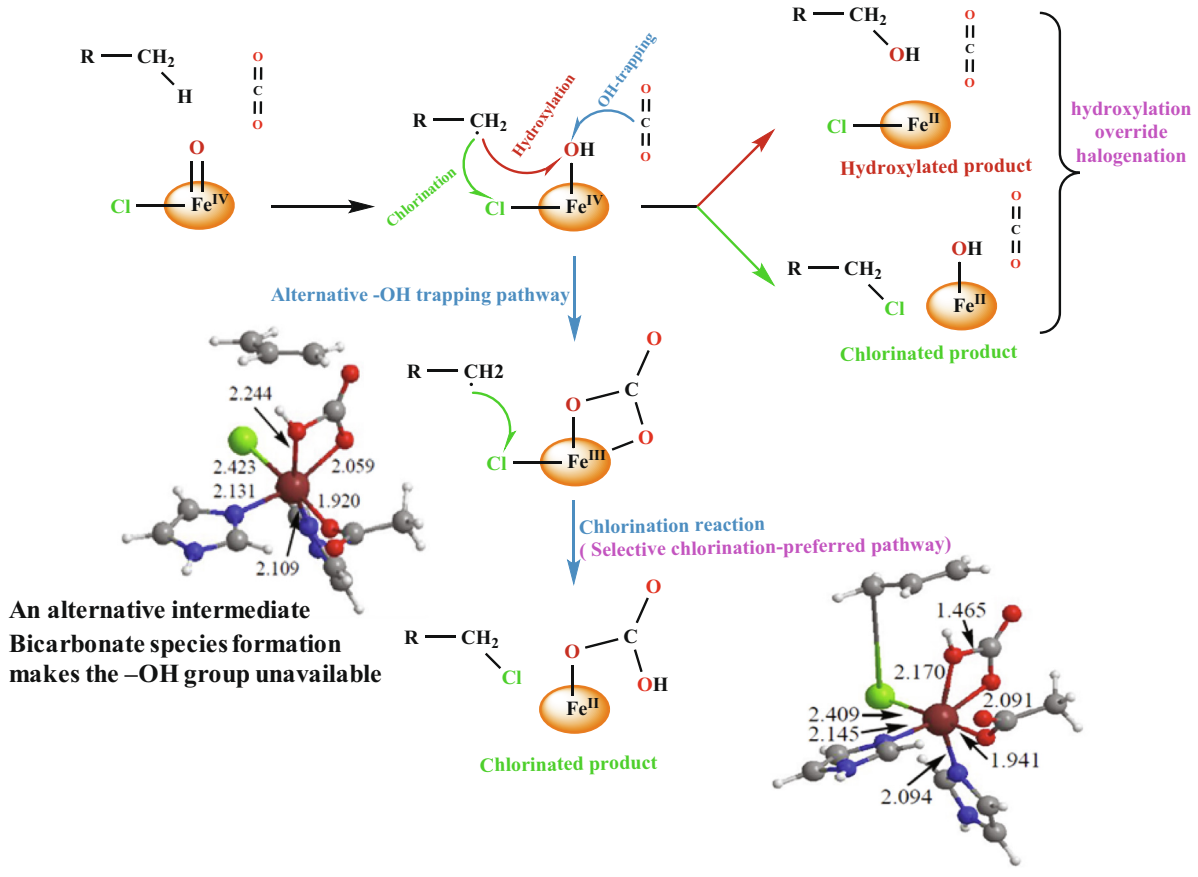

Scheme 10. Schematic representation of the hydroxylation, chlorination and the OH trapping mechanism. Reprinted (adapted) with permission from Ref. [36]. Copyright (2009) American Chemical Society.

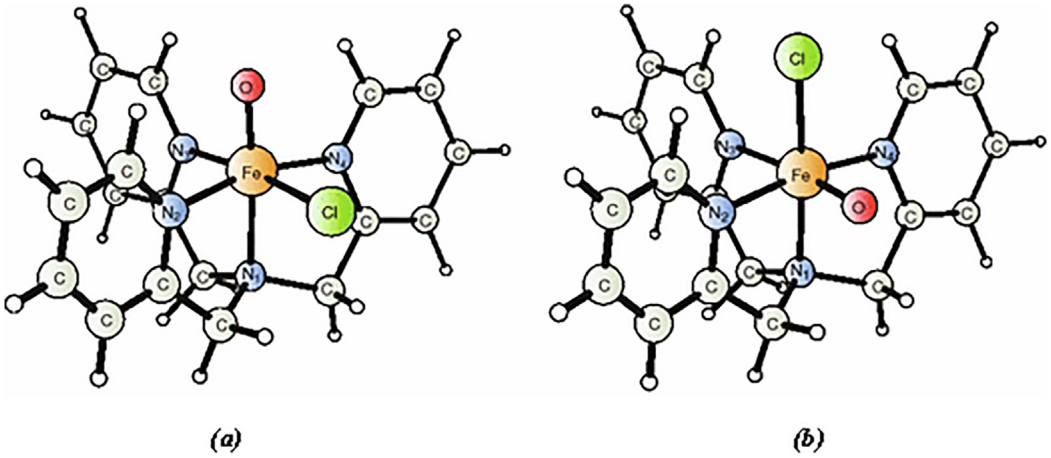

Fig. 16. DFT optimized structure of two isomers, (a) N_{amine} complex where oxygen atom is trans to the axial sp^3 amine nitrogen, (b) $N_{aromatic}$ complex where the chloro group is in trans position of thesp3 amine nitrogen. Reprinted (adapted) with permission from Ref. [120]. Copyright (2007) Springer.

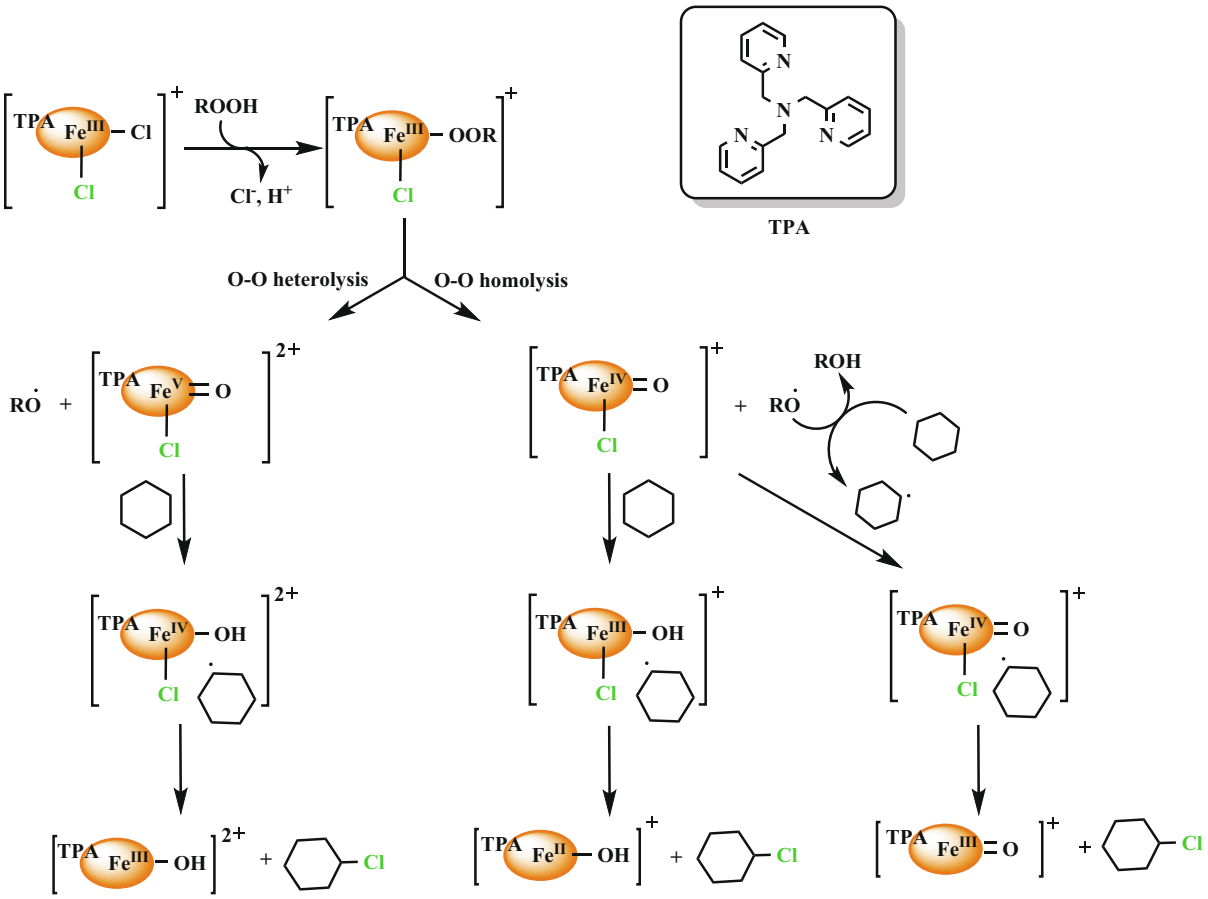

Scheme 11. Probable reaction mechanism of the halogenation of cyclohexane catalyzed by $[(TPA)(Cl_2)Fe^{III}]^+$/RCOOH. Reprinted (adapted) with permission from Ref. [120]. Copyright (2007) Springer.

first step. Measuring the kinetic isotope effect of toluene as the substrate, it is concluded that the C–H bond cleavage takes place initially via hydrogen atom abstraction by $X\text{-}Fe^{IV}{=}O$ complexes. In the following step, an $[(L)(Cl)Fe^{III}\text{-}OH]$ species should be formed with an organic radical system with a solvent cage. The alkyl radical that form may react with the incipient $X\text{-}Fe^{III}\text{-}OH$ species rapidly forming hydroxylated or halogenated products.

The chemoselectivity in the absence of protein environment in these models towards the C-X bond formation is explained by the lower oxidation potentials of the Cl- and Br- ligands (1.36 and 1.07 V respectively) in comparison to OH– ligand (2.02 V). An experimental study has been performed with both TPA and TQA ligand which results in the formation of the halogenated product with comparable selectivity which is indicating to the fact that

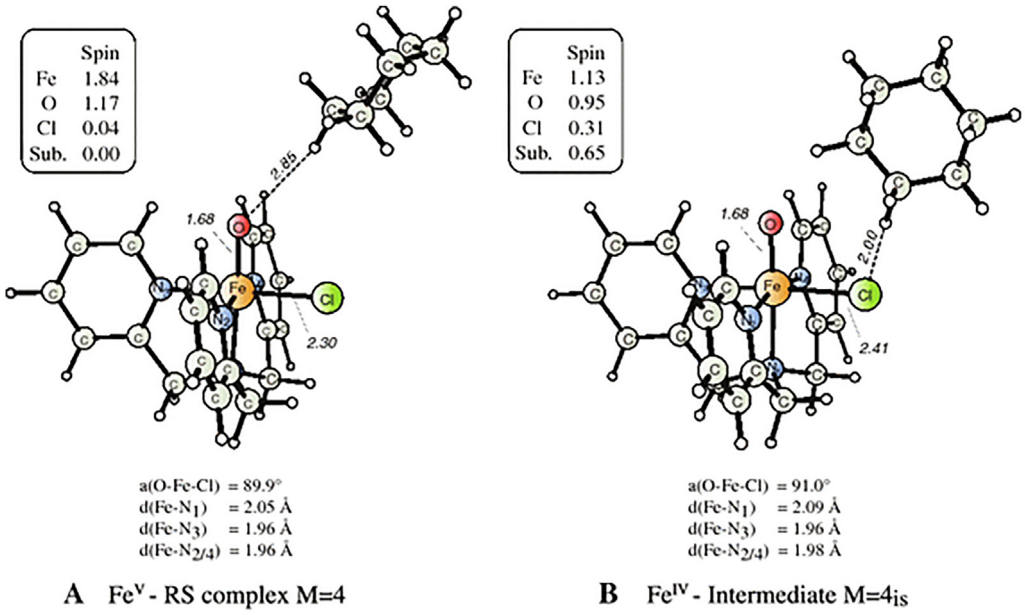

Fig. 17. DFT optimised structures of the transition states for the chlorine rebound on the triplet and quintet potential-energy surfaces. Reprinted (adapted) with permission from Ref. [120]. Copyright (2007) Springer.

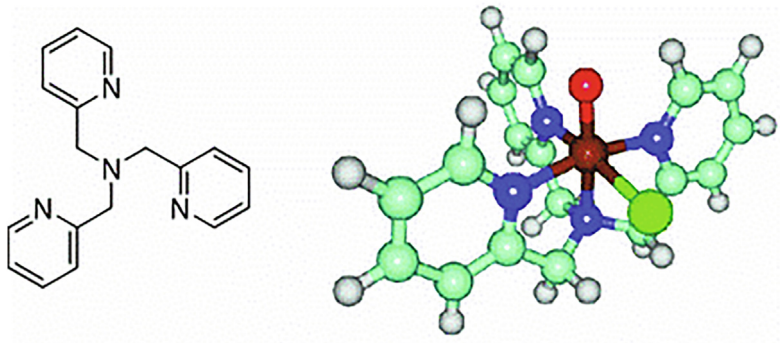

Fig. 18. Chemical structure of the complex $[(TPA)(Cl)Fe^{IV}=O]^+$. Reprinted (adapted) with permission from Ref. [37]. Copyright (2012) Springer.

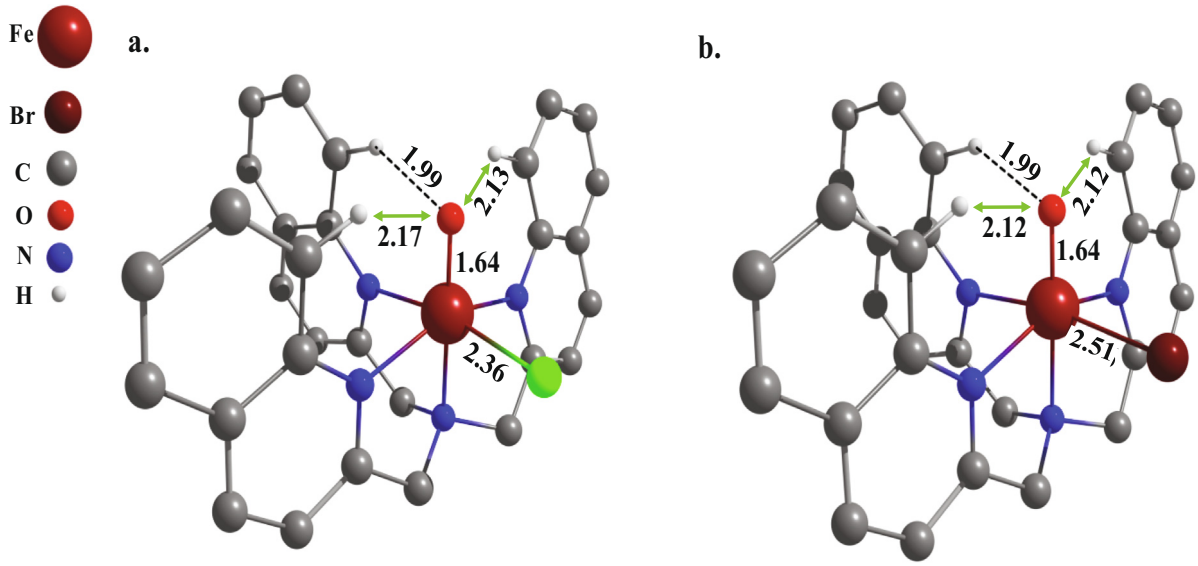

Fig. 19. DFT optimized structure of (a) $[(TQA)(Cl)Fe^{IV}=O]^+$ and (b) $[(TQA)(Br)Fe^{IV}=O]^+$ complexes. Reprinted (adapted) with permission from Ref. [38]. Copyright (2016) American Chemical Society.

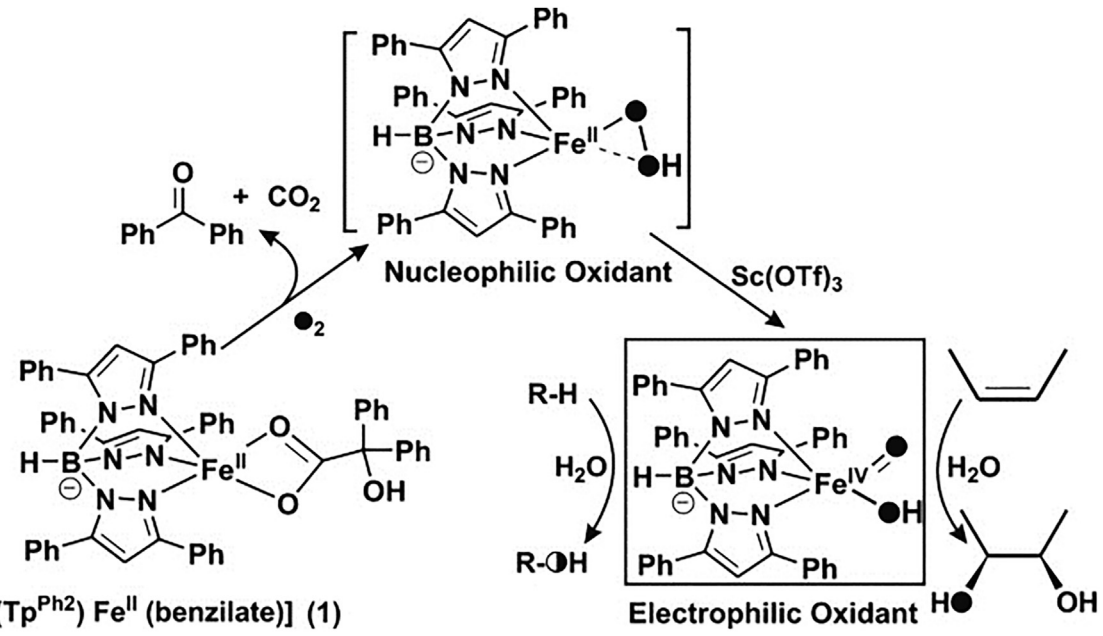

Scheme 12. Proposed reaction mechanism of complex 1 [(Tp^{ph2})Fe^{II}(benzilate)]and O2.Reprinted (adapted) with permission from Ref. [40]. Copyright (2016) Wiley-VCH Verlag GmbH.

increasing the steric bulk of the quinoline donors does not affect the reaction. Therefore, the steric factor does not play an important role here.

Paine and co-workers has explored the reactivity of oxidants containing iron-oxygen system which are generated from an iron (II)-benzilate complex, [(Tp^{ph2})Fe^{II}(benzilate)] [Tp^{Ph2} = hydrotris (3,5-diphenyl-pyrazol-1-yl)borate] via reductive activation of dioxygen [40]. In the preceding oxidative decarboxylation step, iron(II)-hydroperoxy species is generated, which is nucleophilic in nature. Further in this reaction, an HO-Fe^{IV}=O oxidant is formed in the presence of Lewis acid, and this is known to be electrophilic in nature. This can interchange the oxygen atom with H_2O and can perform a wide-ranging variety of selective oxidation reactions. In the presence of Lewis acid, halide ion can promote halogenation reaction to an unactivated aliphatic C–H bond. This complex is another biomimetic model of wild-type halogenase enzyme. The reaction pathway has been shown in Scheme 12.

Recently, Maiti and our group have reported non-heme high-valent iron-oxo complex [(2PyN2Q)Fe^{IV}=O]$^{2+}$, which employ a novel approach for the selective halogenation reaction overriding hydroxylation [41]. In the experimentally proposed mechanism, a pentacoordinated iron(IV)-oxo species [(2PyN2Q)Fe^{IV}=O]$^{2+}$ supported by 2PyN2Q ligand, (1,1-di(pyridin-2-yl)-*N*,*N*-bis(quinolin-2-ylmethyl)methanamine), which is stable at room temperature, is supposed to abstract a hydrogen atom, via HAA (hydrogen atom abstraction) reaction, from the substrate cyclohexane molecule leading to the formation of Fe^{III}-OH intermediate along with the substrate radical in a cage-like structure. After that, there are two possibilities. The first possibility is the –OH rebound where the hydroxyl group was expected to rebound to the carbon radical forming hydroxylated product and the second probability is the escape of the radical from cage leading to the halogenated product (see Scheme 13).

DFT calculation of the putative [(2PyN2Q)Fe^{IV}=O]$^{2+}$ species has predicted S = 1 state as the ground state which is in accord with the previously reported Fe^{IV}=O complexes with pentadentate amino-pyridine ligands like [(2PyN2Q)Fe^{IV}=O]$^{2+}$ [121]. Two-state reactivity is very common in these complexes as excited S = 2 state is close lying to the ground S = 1 state due to the steric and electronic differences in the ligand architecture. In the ground state, the distance between Fe and O atoms is 1.62 Å which is consistent with the previously reported Fe^{IV}=O complexes [27]. The optimized structure of the [(2PyN2Q)Fe^{IV}=O]$^{2+}$ species is shown in Fig. 20.

As compared to the earlier reported Fe^{IV}=O complexes, [(N_4Py)Fe^{IV}=O]$^{2+}$, the –OH rebound barrier is estimated to be significantly high for this complex. The lowest energetic cost of 173.0 kJ/mol (see Fig. 21) at the quintet energy surface for the –OH rebound ruled out the possibility of retention of the cage radical. The important factor that is playing a significant role here is C···H···O interaction between the quinolone C8-H group and the oxygen atom of the –OH group. This restricts the positioning of the –OH hydrogen towards less hindered pyridine rings and forced the substrate radical to approach through the more hindered site, i.e., between the pyridine and quinolone ring which causes a large energy penalty for the –OH rebound and is responsible for the structural deformation of the quinoline moiety. For the previously reported complex, [(N4Py)Fe^{IV}=O]$^{2+}$ the –OH rebound barrier is reported to be 55.2 kJ/mol, which is much lower than this barrier. This section clearly demonstrates that the addition of extra phenyl ring to the pyridine ligand increases the kinetic energy barrier for the hydroxylation reaction.

A very high barrier height for the hydroxylation as compared to chlorination is due to two factors; one is an electronic factor and another is the steric factor, and it is proved that steric factor has played the key role here. This steric factor leads to large deformation energy in the hydroxyl rebound transition state as compared to halogenation. The main reason behind the steric factor is attributed to the Fe^{III}-OH and Fe^{III}-Cl bond lengths. In Fe^{III}-OH species, the cyclohexyl radical has to approach closer to the Fe-centre. This approach causes repulsion from bulky quinoline moieties. Again the energy required for the halogenation process is compensated by the energy gain in the halogen exchange process, which makes the halogenation barrierless.

Although the installation of the carbon [122], oxygen [12,93,123], halogen [32,43] and sulphur [19] to the aliphatic unactivated carbon centre is well-known but enzymatic C-N coupling via the formation of Fe^{IV}=O intermediate is completely unat-

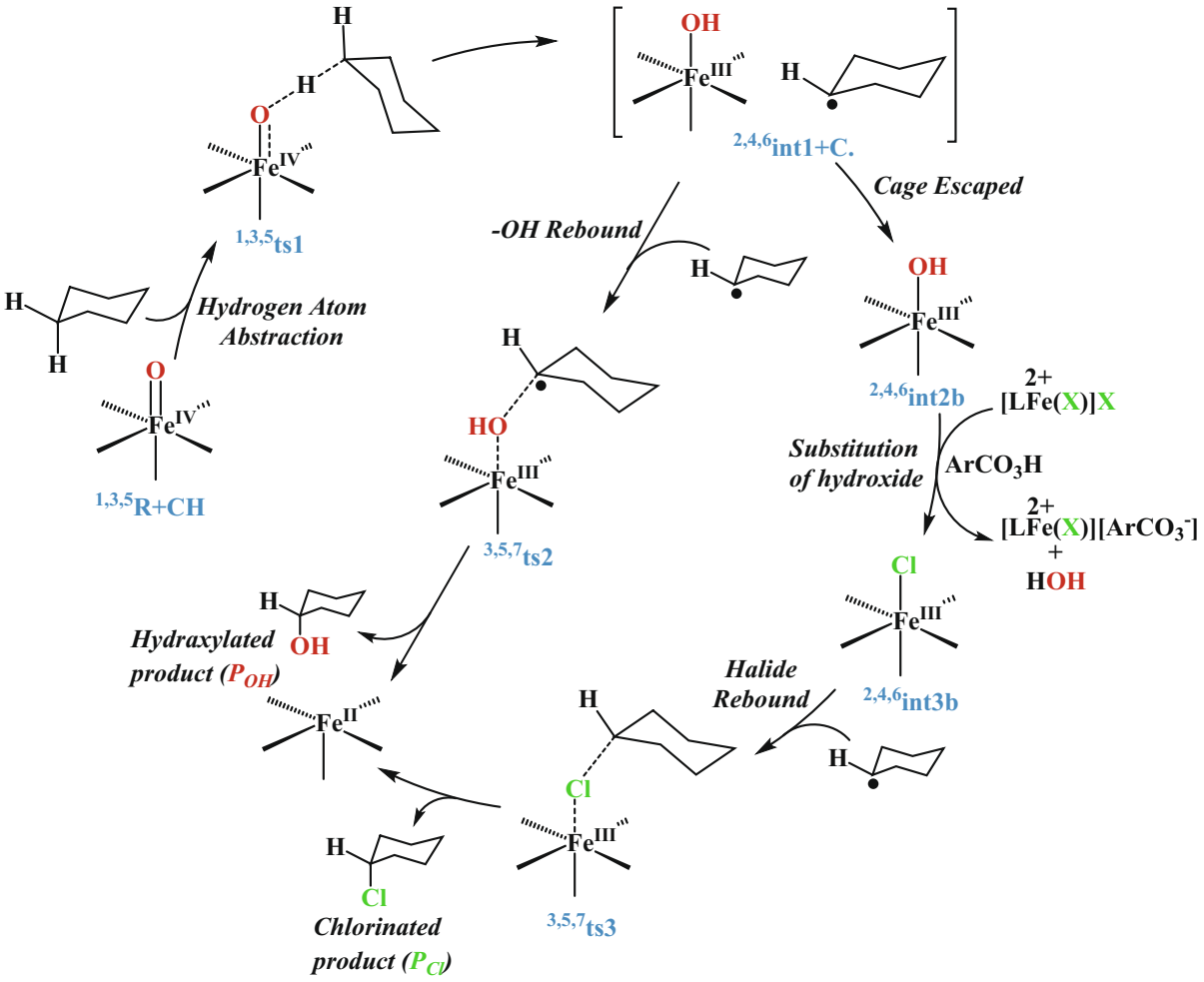

Scheme 13. Mechanistic pathway for the halogenation vs. hydroxylation reaction of cyclohexane by the putative Fe^{IV}=O species. Reprinted (adapted) with permission from Ref. [41]. Copyright (2018) The Royal Society of Chemistry.

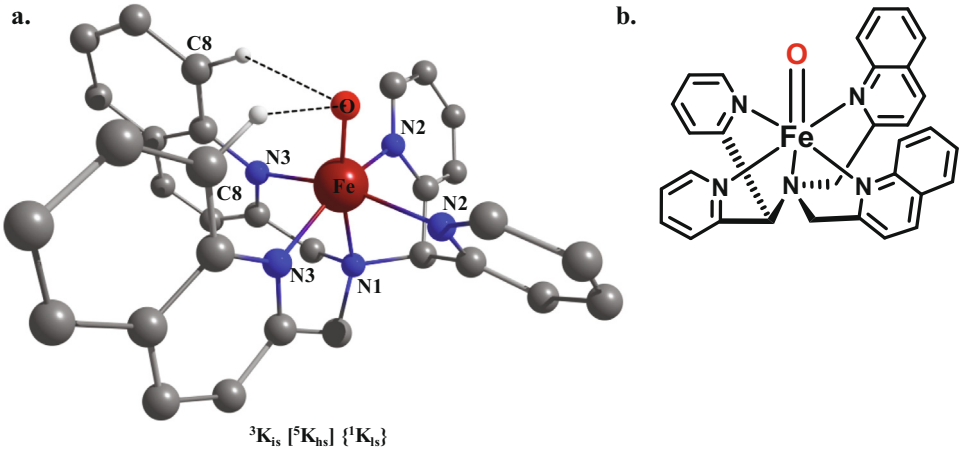

$^3K_{is}$ [$^5K_{hs}$] {$^1K_{ls}$}
r(Fe-O)= 1.626 [1.619] {1.631}
r(Fe-N1)= 2.086 [2.103] {2.084}
r(Fe-N2)= 2.000 [2.132] {2.016}
r(Fe-N3)= 2.036 [2.141] {2.008}
r(C-H...O)= 2.010 [2.110] {2.033}

Fig. 20. (a) DFT optimized structure of $[(2PyN2Q)Fe^{IV}=O]^{2+}$ complex, (b) ChemDraw structure of the Fe^{IV}=O complex. Reprinted (adapted) with permission from Ref. [41]. Copyright (2018) The Royal Society of Chemistry.

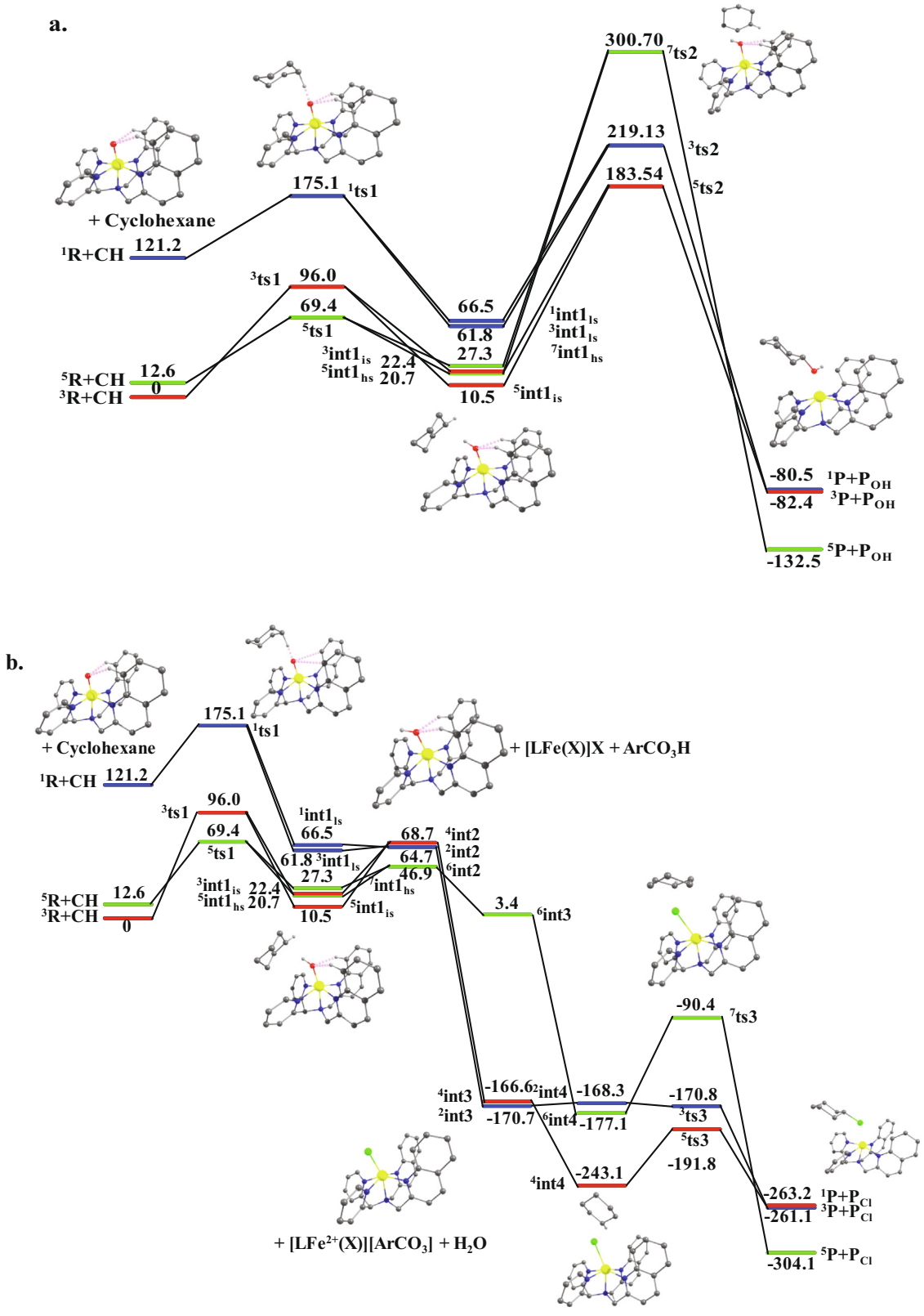

Fig. 21. Potential energy surface diagram for the (a) hydroxylation and (b) halogenation of the cyclohexane as a substrate using $[(2PyN2Q)Fe^{IV}=O]^{2+}$ as catalyst. Energy values are expressed in kJ/mol.Reprinted (adapted) with permission from Ref. [41]. Copyright (2018) The Royal Society of Chemistry.

tempted. Recently, Bollinger Jr. and co-workers have shown that aliphatic nitration and azidation can be directed by the native SyrB2 metalloenzyme in a similar strategy to that of chlorination [42].

5. Comparative oxidative abilities of $LFe^{IV}=O$ vs. $LFe^{IV}=NTs$

While there are several reports on the ways to fine-tune the reactivity and selectivity of the $Fe^{IV}=O$ species such as ligand archi-

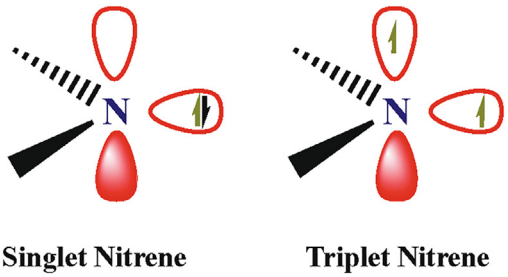

Scheme 14. Schematic diagram of singlet and triplet nitrene.

tecture or presence of axial ligand with better donation capacity, very less has been explored in comparing its oxidizing abilities to the isoelectronic Fe^{IV}-imido species which has the ability to perform similar functions and found to be equally important in biomimetic chemistry. The study of these species gained momentum after the report by Jensen and co-workers in which, for the first time describes the role of an iron(IV)-tosylimide (Fe^{IV}=NTs) species in amination reaction of aromatic compounds via group transfer reaction [124]. Later on, several theoretical studies have been performed to study the aliphatic C–H bond activation by model complexes which confirms the pivotal role played by nitrene nitrogen along with the axial ligand in the reactivity. Eventually, the synthesis and reactivity of Fe^{IV}=NTs species with distinct ligands have been performed by different groups and proved to be potent in hydrogen atom transfer reactions. Que and co-workers attempted to synthesise and characterise the Fe^{IV}=O complex with N_4Py ligand along with the analogues Fe^{IV}=NTs complex and predicted triplet state as a ground state for the $[(N_4Py)Fe^{IV}=NTs]^{2+}$ species [125]. There are two possible spin states, namely singlet and triplet possible for the nitrene group, as shown below (see Scheme 14).

EPR studies on various nitrene complexes confirmed triplet state as a ground state with a very small energy gap (~18 kJ/mol). On complexation with metal ions, nitrene complexes give rise to a complex electronic structure compare to the isoelectronic oxo complexes. In this aspect, a detailed study has been carried out by our group earlier where an attempt has been made to understand the formation energetics of these two species and their electronic and spectral characteristics [126]. DFT studies predict the formation of Fe^{IV}=NTs and Fe^{IV}=O from starting complex $[(N_4Py)Fe^{II}]^{2+}$ (see Fig. 22) and suggest that the formation of nitrene species is thermodynamically favourable with 217.7 kJ/mol, over the generation of corresponding iron-oxo species. The generation of the nitrene species is also found to be a barrierless process.

There are various possible electronic states that arise depending on the spin arrangements in the Fe^{IV} centre viz. S = 0, 1, and 2. For $[(N_4Py)Fe^{IV}=NTs]^{2+}$ there are eight different electronic configurations that are possible due to the combination of four electrons present in the Fe^{IV} centre and two electrons on the nitrogen centre coupled to each other as shown in Fig. 23.

Now if we compare the reactivity of these two species based on the above discussion, the very well-known concept of the TSR comes into the picture. Since the ground state for both the species is predicted to be a triplet, the energy gap between triplet and quintet state will play a crucial role here. In several studies, it is proposed that the quintet state becomes more reactive during the transition state and this study thus underlines the comparative oxidative ability of these two isoelectronic species from bonding picture, though reactivity with some substrates has not been tested at that stage.

Later in 2013, de Visser and co-workers reported the synthesis and comparative oxidative studies on the reactivity of the Fe^{IV}=NTs and Fe^{IV}=O species using N_4Py ligand architecture [127]. In this report, the reactivity of these two species has been tested towards sulfoxidation and HAT reactions. The kinetic studies of sulfoxidation reaction with the thioanisole substrate revealed a much higher rate constant for nitrene species than the corresponding oxo species. Surprisingly, a reverse trend has been observed for the HAT reaction where Fe^{IV}=O species is found to be better oxidant than Fe^{IV}=NTs species. To solve this mystery, theoretical tools have been used to shed light on the reactivity trend and mechanism. Calculations have been performed on the two different substrates viz. DMS (dimethylsulphide) and CHD (cyclohexadiene) for the sulfoxidation and HAT reaction, respectively.

DFT analysis suggests a one-step mechanism for the sulfoxidation reaction while it becomes two steps when it comes to HAT reaction. For HAT reaction, the first step is found to be the rate-determining step, followed by another hydrogen atom abstraction by the radical intermediate to give the product. Among these

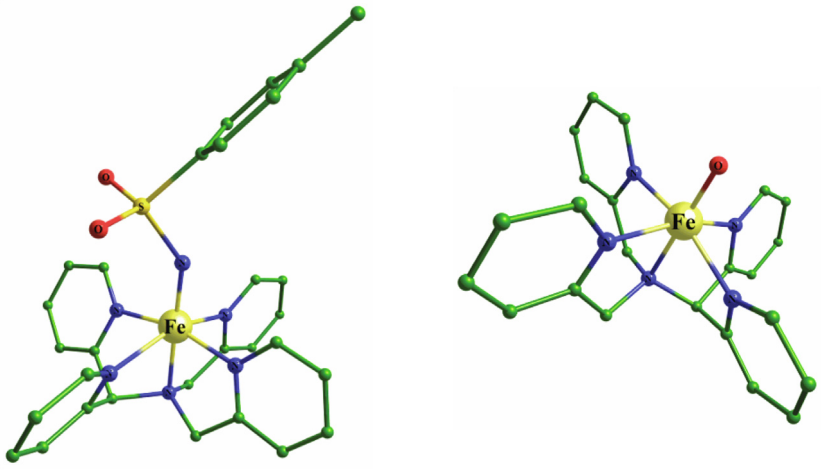

Fig. 22. Optimized structures of the ground state (a) $[N_4Py)Fe^{IV}=NTs]^{2+}$ and (b)$[(N_4Py)Fe^{IV}=O]^{2+}$.

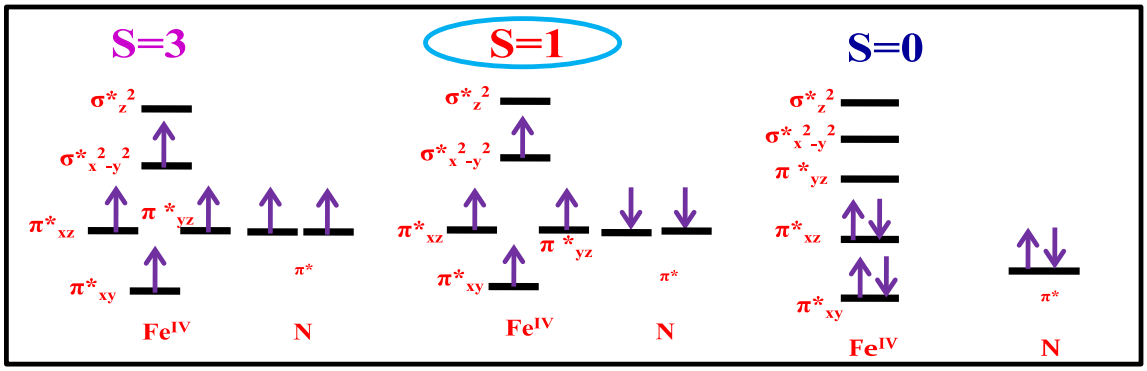

	Electronic Configuration
S=3	$\delta^{\uparrow}\ \pi^{*\uparrow}_{xz}\ \pi^{*\uparrow}_{yz}\ \sigma^{*\uparrow}\ \delta\quad \varphi_{N1}^{\uparrow}\ \varphi_{N2}^{\uparrow}$
S=1	$\delta^{\uparrow}\ \pi^{*\uparrow}_{xz}\ \pi^{*\uparrow}_{yz}\ \sigma^{*\uparrow}\ \delta\quad \varphi_{N1}^{\downarrow}\ \varphi_{N2}^{\downarrow}$
S=2	$\delta^{\uparrow\downarrow}\ \pi^{*\uparrow}_{xz}\ \pi^{*\uparrow}_{yz}\ \sigma^{*}\ \delta\quad \varphi_{N1}^{\uparrow}\ \varphi_{N2}^{\uparrow}$
S=0	$\delta^{\uparrow\downarrow}\ \pi^{*\uparrow}_{xz}\ \pi^{*\uparrow}_{yz}\ \sigma^{*}\ \delta\quad \varphi_{N1}^{\downarrow}\ \varphi_{N2}^{\downarrow}$
S=1	$\delta^{\uparrow\downarrow}\ \pi^{*\uparrow\downarrow}_{xz}\ \pi^{*}_{yz}\ \sigma^{*}\ \delta\quad \varphi_{N1}^{\uparrow}\ \varphi_{N2}^{\uparrow}$
S=2	$\delta^{\uparrow}\ \pi^{*\uparrow}_{xz}\ \pi^{*\uparrow}_{yz}\ \sigma^{*\uparrow}\ \delta\quad \varphi_{N1}^{\uparrow\downarrow}\ \varphi_{N2}$
S=1	$\delta^{\uparrow\downarrow}\ \pi^{*\uparrow}_{xz}\ \pi^{*\uparrow}_{yz}\ \sigma^{*}\ \delta\quad \varphi_{N1}^{\uparrow\downarrow}\ \varphi_{N2}$
S=0	$\delta^{\uparrow\downarrow}\ \pi^{*\uparrow\downarrow}_{xz}\ \pi^{*}_{yz}\ \sigma^{*}\ \delta\quad \varphi_{N1}^{\uparrow\downarrow}\ \varphi_{N2}$

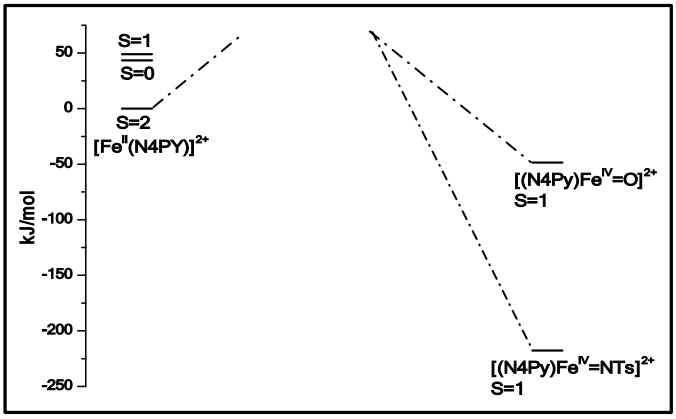

Fig. 23. Electronic configurations for various possible spin state and comparative energy profile diagram for the formation of $[(N_4Py)Fe^{IV}{=}O]^{2+}$ and $[(N_4Py)Fe^{IV}{=}NTs]^{2+}$. Reprinted (adapted) with permission from Ref. [126]. Copyright (2012) The Royal Society of Chemistry.

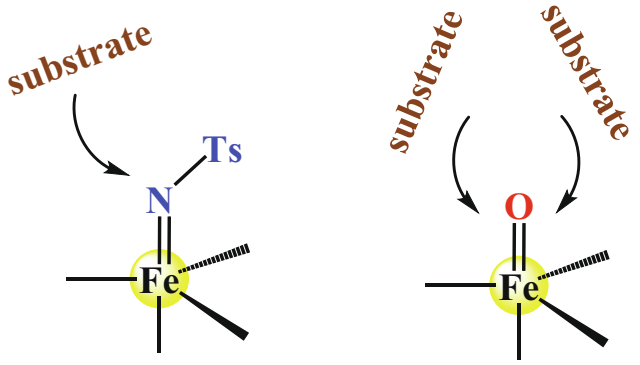

Fig. 24. Schematic representation for accessible sites for the attack of the substrate for Fe^{IV}=NTs (left) and Fe^{IV}=O (right).

species, the $[(N_4Py)Fe^{IV}{=}O]^{2+}$ is predicted to be a better oxidant than $[(N_4Py)Fe^{IV}{=}NTs]^{2+}$ for HAT reaction. Although the sulfoxidation reaction catalysed by these species is calculated to be concerted, the electronic nature of the transition state is not similar. Higher charge transfer from substrate to the oxidant has been observed for the sulfoxidation transition states (for triplet and quintet spin states both) of the species $[(N_4Py)Fe^{IV}{=}NTs]^{2+}$, hence is confirmed as a product like transition state. In contrast to the transition states of the species $[(N_4Py)Fe^{IV}{=}O]^{2+}$, this is assigned as a reactant like or early transition state. The calculated electronic affinity values also predict the species Fe^{IV}=NTs acts as a better electrophile than Fe^{IV}=O species. In both cases, the reactant species are stabilized in the triplet state but in the transition state, the quintet spin state becomes the ground state [128]. Due to the presence of a bulky tosylate group, which imparts angle constraints, the oxidant can offer only accessible site to the substrate, i.e. the opposite side of the tosylate group. This snips the possibility of transfer of electrons to the σ^{*2}_{dz} orbital, indicating the involvement of π orbitals (π pathway). Which pathway will be followed by the oxidant is dependent on the ease of approachability of the orbitals. Here, in particular, for $[(N_4Py)Fe^{IV}{=}NTs]^{2+}$ species only one site is accessible for the substrate while for the $[(N_4Py)Fe^{IV}{=}O]^{2+}$ species the substrate can approach from either of the sides (see Fig. 24).

Hence, Fe^{IV}=NTs species reacts via π-pathway in contrast to the Fe^{IV}=O species which reacts via σ-pathway. This leads to species $[(N_4Py)Fe^{IV}{=}NTs]^{2+}$ to possess a higher barrier height than species $[(N_4Py)Fe^{IV}{=}O]^{2+}$. Although both these species are possessing similar electronic ground state, $[(N_4Py)Fe^{IV}{=}NTs]^{2+}$ acts as a better oxidant for sulfoxidation reaction in contrast to $[(N_4Py)Fe^{IV}{=}O]^{2+}$ which unbeatably a good oxidant for HAT reactions. The reason stated behind this reactivity trend is stereochemical repulsion. To summarize the reactivity of species $[(N_4Py)Fe^{IV}{=}NTs]^{2+}$ and $[(N_4Py)Fe^{IV}{=}O]^{2+}$, we can say the stronger electron affinity of species $[(N_4Py)Fe^{IV}{=}NTs]^{2+}$ makes it better oxidant in sulfoxidation reaction which proceeds via a concerted step in contrast to the HAT reaction which is a one-electron transfer reaction. The leading cause of reactivity differences between the two species is still not clear. Later, in another follow-up report by the same group [129] further reactivity of species $[(N_4Py)Fe^{IV}{=}NTs]^{2+}$and $[(N_4Py)Fe^{IV}{=}O]^{2+}$ have been explored. The effect of electron affinity on the reactivity on the basis of different valence orbital shapes has been discussed.

Collectively on the basis of the above experimental results, it can be concluded that the mechanism of Fe^{IV}=O species involves group transfer with sulfides while Fe^{IV}=NTs species undergoes electron transfer reaction. Further, DFT methods have been used to investigate the nature and reactivity trends in detail. Like earlier reports, here also DMS (dimethylsulphide) and CHD (cyclohexadiene)/benzyl alcohol have been used as the substrates to perform

sulfoxidation or HAT reactions, respectively. Calculations predict no change in the spin state ordering of these two species $[(N_4Py)Fe^{IV}{=}O]^{2+}$ and $[(N_4Py)Fe^{IV}{=}NTs]^{2+}$.

The major difference observed is the interaction between iron $3d_{xz}$ orbitals with not only the nitrogen but with the σS—N bonding orbital to form π_{xz}/π^*_{xz} set of orbitals which is absent in Fe^{IV}=O species. In Fe^{IV}=O species the $3d_{xz}$ and $3d_{yz}$ orbitals on iron interact with $2p_x/2p_y$ orbitals on the oxo group gives rise a degenerate pair of π_{xz}/π^*_{xz} and π_{yz}/π^*_{yz} and this degeneracy is lifted in Fe^{IV}=NTs species due to the presence of tosyl group. A combination of $3d_z^2$ and $2p_z$ orbitals results in the σ^{*2}_z orbital in species $[(N_4Py)Fe^{IV}{=}O]^{2+}$. In species $[(N_4Py)Fe^{IV}{=}NTs]^{2+}$, the interaction not only involves $3d_z^2$ orbital on Fe and $2p_y$ on N orbitals but also $3p_z$ of S orbital. This affects the orbital energies drastically leads the change in σ^{*2}_z and $\sigma^*d^2_{xy}$ ordering of the orbitals. This alteration in orbital arrangements reduces the HOMO-LUMO gap in species $[(N_4Py)Fe^{IV}{=}NTs]^{2+}$, hence increases the electrophilicity. This is the reason behind the different reactivity patterns observed.

One of the interesting observations during the HAT with Fe^{IV}=NTs species is that the calculated values predict the transfer of an electron from the substrate to the Fe^{IV}=NTs at a relatively long distance in the reactant complex. At this early stage itself metal centre gets reduced by one electron and as a consequence of that substrate becomes a cation radical. This infers that instead of $[(N_4Py)Fe^{IV}{=}NTs]^{2+}\cdots$CHD, the existing complex is $[(N_4Py)Fe^{III}\text{-}NTs]^{+}\cdots CHD^{+\bullet}$, and considered as to be a real oxidant (see Scheme 15). This can be explained by the greater electron affinity of the Fe^{IV}=NTs species, which leads to electron transfer even before the substrate activation, i.e. the first step. Previous reactivity studies on the $[(N4Py)Fe^{IV}{=}NTs]^{2+}$ indicate five unpaired electrons on the iron centre which antiferromagnetically coupled to a radical intermediate [128]. Considering the electronic configuration, the major difference arises due to one-electron transfer in the formation of long-range reactant complex R, leading to a triplet ground state with an electronic configuration of $\pi^{*2}_{xy}\pi^{*2}_{xz}\pi^{*1}_{xz}\pi^{1}_{CHD}$, resembling $[(N_4Py)Fe^{III}(NTs)]^{+}\cdots CHD^{+\bullet}$ Complex. Further addition of an electron to the complex gives [(N4Py)Fe^{II}-(NHTs)] intermediate as shown in Scheme 15.

In conclusion of this part, we can say that Fe^{IV}=O acts as a better oxidant in HAT while Fe^{IV}=NTs species acts faster in heteroatom oxidation, i.e. sulfimidaion reaction. Due to higher electron affinity values of Fe^{IV}=NTs, it accepts electron at longer distance and forms Fe^{III}-NTs species, which perform the HAT reaction. This is not applicable to Fe^{IV}=O species. For the sulfoxidation reaction, the two-electron transfer takes place to the Fe^{IV}=NTs centre while the one-electron transfer takes place to the Fe^{IV}=O centre. These findings prove Fe^{IV}=O species is a better oxidant for HAT reactions while Fe^{IV}=NTs is a better oxidant for heteroatom transfer reaction, which is also in agreement with the BDEs and EA concepts discussed before. As the HAT is governed by the BDEs while heteroatom transfer with EA [44].

Till then all the studied have been carried out on intermolecular reactions. Later in 2017, our group reported a detailed study of intramolecular amination/hydroxylation reactions by these Fe^{IV}=NTs species and Fe^{IV}=O species [130]. The $[(6\text{-Ph-TPA})Fe^{IV}{=}NTs]^{2+}$ and $[(6\text{-Ph-TPA})Fe^{IV}{=}O]^{2+}$, species have been synthesized by the reaction of $[(6\text{-Ph-TPA})Fe^{II}]^{2+}$ with PhINTs/PhIO species. The work was inspired by a report published in 2003, by Que and coworkers about the intramolecular amination/hydroxylation reaction by $[(6\text{-Ph-TPA})Fe^{IV}{=}X]^{2+}$ (where X = NTs, O) [124]. The $[(6\text{-Ph-TPA})Fe^{IV}{=}NTs]^{2+}$ and $[(6\text{-Ph-TPA})Fe^{IV}{=}O]^{2+}$ species are proposed as a potent oxidant in intramolecular amination and hydroxylation reaction, respectively. For this particular reaction, the nitrene species were reported to be superior to the corresponding oxo analogues, which area well-known oxidant in various reactions. A comparative study of the mechanism for intramolecular amination/hydroxylation reaction by $[(6\text{-PhTPA})Fe^{IV}{=}NTs]^{2+}$ and $[(6\text{-PhTPA})Fe^{IV}{=}O]^{2+}$ is shown in Fig. 25 (only the lowest energy points have been shown). The calculated barrier height for the first electrophilic attack is found to be lower for Fe^{IV}=NTs species than the corresponding Fe^{IV}=O species (25.9 vs. 54.6 kJ/mol for Fe^{IV}=NTs and Fe^{IV}=O, respectively, this step is predicted to be the rate-determining step). Our results affirm that Fe^{IV}=NTs species is found to be more reactive than the corresponding Fe^{IV}=O species in an *ortho*-hydroxylation reaction similar to the sulfoxidation reaction. But surprisingly Fe^{IV}=O species was known to be a potent oxidant. This fascinated us to do perform additional studies on the HAT reactions on DHA substrate. A similar trend is observed as reported previously [128,129] for HAT reaction where Fe^{IV}=NTs species found to be a sluggish oxidant. Analysing transition states for both the reactions, it has been found that the Fe—X—Y (X = NTs/O; Y = C/H) angle is playing an important role. The calculated Fe—NTs—C and Fe—O—C angles are found to be nearly 105° and 117°, respectively. Both the angle values are less than 120° confirms π-pathway is the only possible pathway for intramolecular reaction due to constraints in angle. On the other hand, for HAT reactions, there is a geometry constraint for the Fe^{IV}=NTs species due to the presence of bulky tosylate group (pointing involvement of π-pathway) but for Fe^{IV}=O the substrate can approach from either side either π or σ –pathway. For HAT reactions, the Fe—NTs—H and Fe—O–H angles are calculated to be nearly 117° and 168°, respectively. This suggests π-pathway and σ pathway for Fe^{IV}=NTs and Fe^{IV}=O, species, respectively.

Analysing the nature of the transition state for the two reactions confirmed that whenever there is a possibility of two-electron transfer, undoubtedly Fe^{IV}=NTs becomes the stronger oxidant due to additional flexibility available in the structure of the Fe^{IV}=NTs species. For a one-electron transfer reaction, it behaves as a sluggish oxidant. Thus the geometry constrained on Fe^{IV}=NTs suggests that this can undergo only π-pathway while the isoelectronic

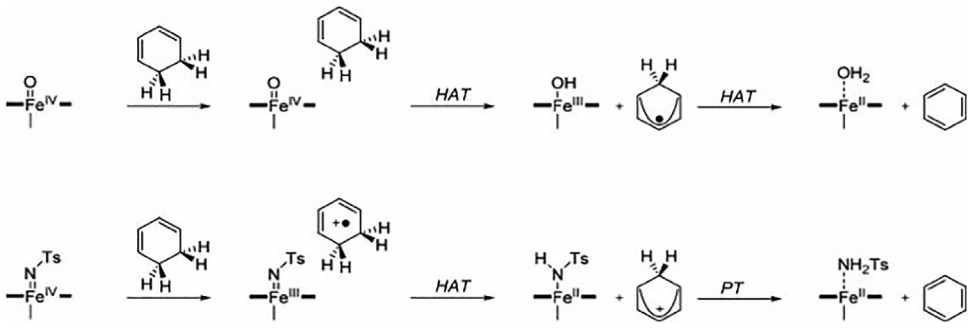

Scheme 15. Proposed reaction mechanisms for Fe^{IV}=O and Fe^{IV}=NTs complexes on the basis of group spin density plots. Reprinted (adapted) with permission from Ref. [129]. Copyright (2014) American Chemical Society.

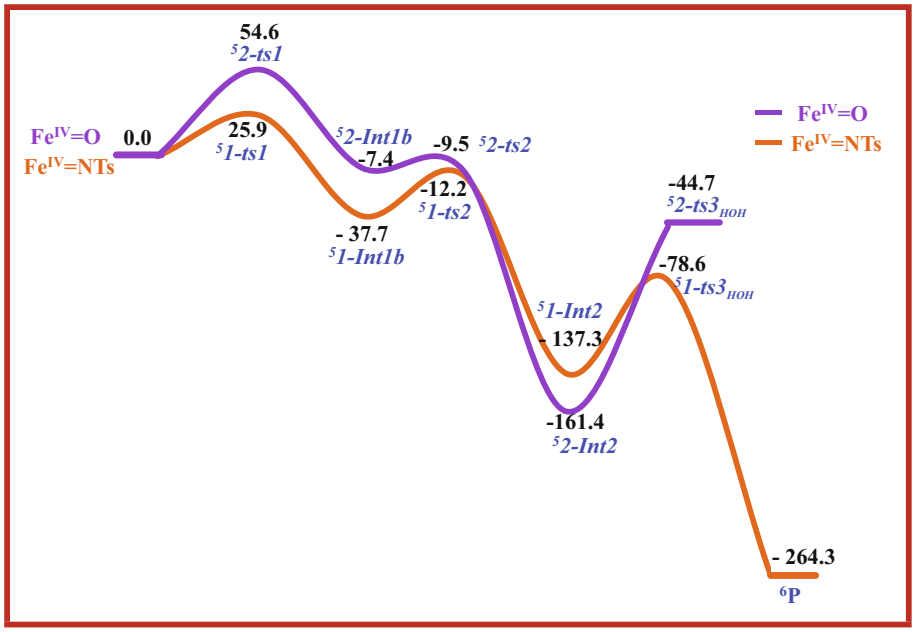

Fig. 25. B3LYP computed free energy profile (ΔG in kJ/mol) of intramolecular amination and hydroxylation by $[(6\text{-PhTPA})Fe^{IV}{=}NTs]^{2+}$ and $[(6\text{-PhTPA})Fe^{IV}{=}O]^{2+}$.Reprinted (adapted) with permission from Ref. [130]. Copyright (2012) The Royal Society of Chemistry.

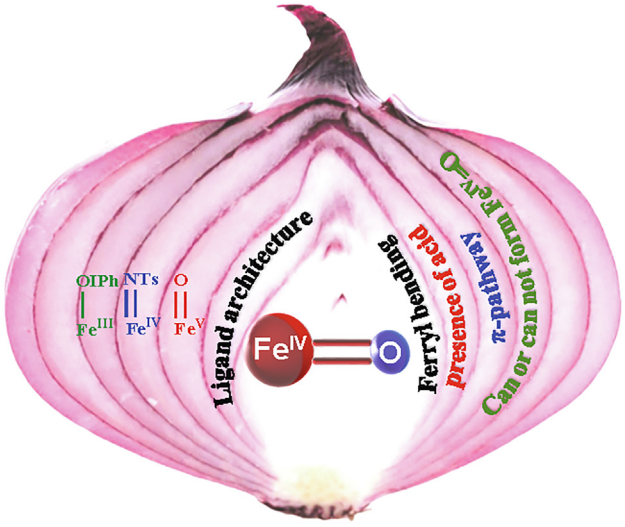

Scheme 16. A schematic representation of various degrees of freedom that has been altered to understand the comparative oxidative ability of the popular non-heme Fe^{IV}=O unit.

Fe^{IV}=O can undergo π-pathway as well as σ–pathway, depending on the nature of the reaction/substrate.

6. Conclusions

There is a growing interest to understand the reactivity of the popular Fe^{IV}=O as they play a key role in the reactivity of various metalloenzymes. Theoretical tools are indispensable in this area as they offer a unique set of understanding of the mechanistic aspects of various biomimetic models. While several reviews on this topic has been written already, here we intend to understand the comparative oxidative ability of the popular Fe^{IV}=O species by subjecting it to various degrees of freedom such as (i) alteration in the oxidation state (ii) variation in the equatorial ligands (iii) altering the ligand architecture to test the reactivity towards chemoselectivity (iv) substituting the ferryl-oxygen by isoelectronic NTs species. The most important point that is derived from these reviews is schematically shown in Scheme 16 as a layer of the onion to understand fully the intrinsic reactivity of Fe^{IV}=O species finally. The detailed explanation for each of the points shown in Scheme 16 is summarised below.

In the first part of the review, we have discussed the involvement of various oxidation states on the iron in different reaction conditions. A study of the *ortho*-hydroxylation of aromatic compounds using a catalyst precursor $[(TPA)Fe^{II}(CH_3CN)_2]^{2+}$ in the presence of H_2O_2 explores the reactivity pattern of the iron complex in different oxidation states. DFT study confirms that the formation of Fe^{III}-OOH via direct attack of the distal and proximal oxygen to the aromatic carbon atom in the *ortho*-position is ruled out as this path is associated with very high barrier heights. The formation of Fe^{IV}=O and Fe^{V}=O via homolytic and heterolytic cleavage of the O···O bond finds to be energetically favourable, and further calculation suggests Fe^{V}=O species as a more potent oxidising agent than that of Fe^{IV}=O species due to less barrier associated with the substrate activation. Moreover, another study has been performed to check on the reactivity of the Fe^{V}=O species in the presence of different ligand environment. The higher reactivity of the $[(BPMEN)(C_6H_5COO)Fe^{V}{=}O]^{2+}$ complex than that of the $[(TPA)(C_6H_5COO)Fe^{V}{=}O]^{2+}$ is a result of the subtle difference in the ligand architecture that stabilises the $\pi^*_{Fe=O}$ orbitals that play a key role in the reactivity. In the preceding section, the comparative oxidative ability of the Fe^{IV}=O/Fe^{V}=O species and their precursor complex $Fe^{II/III}$-OX (X = IPh, OH, and OR) have been discussed. This section highlights the anomaly that if the I···O bond is not cleaved or half-cleaved, this does not necessarily generate the desired Fe^{IV}=O species. Various studies suggest that these species are also on the race for the reactivity observed and ligand architecture plays a critical role here in dictating the formation of the putative Fe^{IV}=O species. As mentioned earlier that the increase in the oxidation state results in an enhanced electrophilicity of metal which in turn enhances the ability to abstract a proton. This observation suggests an increase in the BDE of Fe-OH bond and a decrease in the barrier height. But sometimes the formation of the high-valent Fe^{IV}=O/Fe^{V}=O species is thermodynamically and kinetically

not favourable and in this scenario, the precursor complex itself may have enough electrophilicity to oxidize the substrate (see Box 1, below).

aspect of the naturally occurring wild type Fe(II)-α-KG dependent halogenase metalloenzyme which can selectively transfer halogen atom to the unactivated aliphatic C–H bonds was compared. The

Take home messages

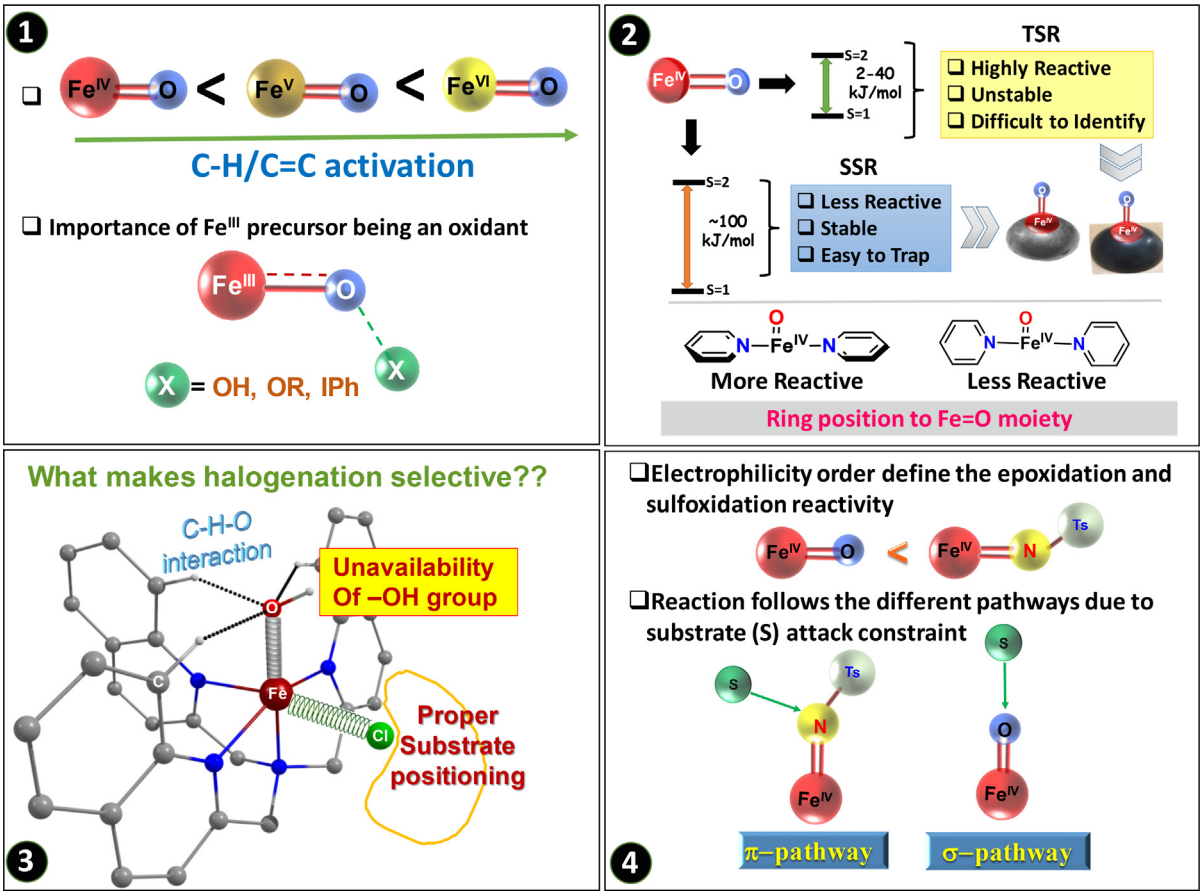

From DFT calculations, the conclusions have been derived that decreasing the ligand field of the axially attached ligands to the Fe^{IV}=O systems leads to greater accessibility of the reactive S = 2 spin state increasing the reactivity. The main reason behind this fact that, decreasing anionic ligand strength destabilise d_z^2 and $d_{xz/yz}$ orbitals and stabilise the $d_{x^2-y^2}$ orbital leading to the decrease in the energy gap between quintet and triplet spin state and increase the mixing of the S = 2 state. Equatorial ligands play a crucial role in the selectivity of the Fe^{IV}=O complexes by effecting the redox potentials of the systems. A very strong equatorial ligand attached to the Fe^{IV}=O moiety can decrease the hydrogen atom abstraction rate by lowering the energy of d_{xy} orbitals in comparison to $d_{x^2-y^2}$ orbitals. Again, it is established that in the presence of a strong σ-donating ligand, axial ligands are not much influence the reactivity of the metal-oxo system, and they exhibit pure triplet state reactivity (see Box 2, below).

In the forthcoming section, the role of ligand architecture on the chemoselectivity was discussed. In this part, the mechanistic

active species involved in these systems is Fe^{IV}=O which can effectively activate the aliphatic C–H bond, and in the preceding step the halogen atom migrates to the carbon centre leading to the halogenated product. DFT calculations on the enzymatic model systems have established the fact that substrate positioning plays an important role in the product selectivity. In addition to this, it has been observed that the hydrogen bonding between the ligands attached to the Fe-centre plays an important role in selectivity by lowering the energy of the transition state corresponding to the halogenation. Another explanation for the selectivity towards halogenation is described by the fact that the evolved CO_2 in one of the steps in the reaction mechanism interacts with the –OH group making it unavailable for the hydroxylation reaction.

Further, based on the knowledge gained from experimental and theoretical studies on the native enzymes, several experimental research groups are involved in the design of biomimetic models of these naturally occurring metalloenzymes. Their main purpose is to develop a structural analogue of the naturally occurring pro-

tein to mimic the chemoselectivity in the laboratory. Unfortunately, over the decades, the main hurdle in this way was to achieve the desired selectivity. Most efforts were undertaken earlier lead to a mixture of products. Slowly over time, improvements have been performed in the ligand design, and in the last few years, a significant breakthrough has been achieved. The key here is enhancing the bulkiness of the ligand architecture, which in turn enhance the barrier height for the rebound pathway leading to chemoselectivity. Another important point to mention here is the ferryl bend where L-Fe=O angle is found to bend aiding HAT abstraction significantly and at the same time hindering rebound pathway. Based on all the reported data in this area, we can conclude by saying that the ligand environment plays an essential role to achieve the selectivity by i) increasing the steric hindrance, which facilitates the halogen atom transfer ii) altering the redox potential of the systems iii) by orienting the substrate in such a way that halogen atom transfer is favoured (see Box 3, below).

The last section in this review is the comparison of the oxidising power of the Fe^{IV}=O species with the Fe^{IV}=NTs system. DFT calculations on both the species prove that they possess a triplet state as the ground state and potent in hydrogen atom transfer reactions. The presence of a large tosylate group attached to the N-centre is responsible for the comparative elongation of the Fe-NTs bond length than that of the Fe-O bond, which is the key reason for the high reactivity of the Fe^{IV}=NTs complexes. In the case of Fe^{IV}=NTs, the bulky tosylate group limits the approach of the substrate molecule from the opposite side of the tosylate group preventing the transfer of electrons to the σ^{*2}_{dz} which leads to the involvement of only π orbitals. On the other hand, in the case of Fe^{IV}=O species, the substrate can be able to approach from both the side leading to the involvement of σ-orbitals. While Fe^{IV}=NTsundergoes π-pathway, Fe^{IV}=O undergoes σ-pathway (see Box 4, below).

Declaration of Competing Interest

The authors declare that they have no known competing financial interests or personal relationships that could have appeared to influence the work reported in this paper.

Acknowledgements

We thank the Science and Engineering Research Board and Department of Science and Technology (CRG/2018/000430; DST/SJF/CSA-03/2018-10; SB/SJF/2019-20/12) New Delhi, for financial support of this research. A computational facility at Indian Institute of Technology Bombay is greatly acknowledged. RK and AS thank CSIR for an SRF fellowship. BP and SS would like to acknowledge UGC for the grant. MA would like to thanks IIT Bombay for funding.

Appendix A. Supplementary data

Supplementary data to this article can be found online at https://doi.org/10.1016/j.ccr.2020.213397.

References

[1] L. Que Jr., R.Y.N. Ho, Chem. Rev. 96 (1996) 2607–2624.
[2] B. Meunier, Biomimetic Oxidations Catalyzed by Transition Metal Complexes, Imperial College Press, London, 2000.
[3] M.T. Green, Curr. Opin. Chem. Biol. 13 (2009) 84–88.
[4] W. Zhang, J.L. Loebach, S.R. Wilson, E.N. Jacobsen, J. Am. Chem. Soc. 112 (1990) 2801–2803.
[5] K. Srinivasan, P. Michaud, J.K. Kochi, J. Am. Chem. Soc. 108 (1986) 2309–2320.
[6] M. Palucki, N.S. Finney, P.J. Pospisil, M.L. Güler, T. Ishida, E.N. Jacobsen, J. Am. Chem. Soc. 120 (1998) 948–954.
[7] P.R. Ortiz de Montellano, Chem. Rev. 110 (2010) 932–948.
[8] N. Jin, J.T. Groves, J. Am. Chem. Soc. 121 (1999) 2923–2924.
[9] J.T. Groves, J. Lee, S.S. Marla, J. Am. Chem. Soc. 119 (1997) 6269–6273.
[10] E.J. Mueller, P.J. Loida, S.G. SLiga, Cytochrome P450: Structure, Mechanism and Biochemistry, second ed., Plenum Press, New York, 1995.
[11] M. Fontecave, S. Ménage, C. Duboc-Toia, Coord. Chem. Rev. 178–180 (1998) 1555–1572.
[12] C. Krebs, D.G. Fujimori, C.T. Walsh, J.M. Bollinger Jr., Acc. Chem. Res. 40 (2007) 484–492.
[13] M.M. Abu-Omar, A. Loaiza, N. Hontzeas, Chem. Rev. 105 (2005) 2227–2252.
[14] M. Costas, K. Chen, L. Que Jr., Coord. Chem. Rev. 200 (2000) 517–544.
[15] R.A. Sheldon (Ed.), Metalloprophyrins in Catalytic Oxidations, Marcel Dekker, New York, 1994.
[16] P.R. Ortiz de Montellano, Cytochrome P450: Structure, Mechanism, and Biochemistry, third ed., Springer, Berlin, 2005.
[17] S. Shaik, W. Lai, H. Chen, Y. Wang, Acc. Chem. Res. 43 (2010) 1154–1165.
[18] W. Nam, J.S. Valentine, J. Am. Chem. Soc. 115 (1993) 1772–1778.
[19] J.E. Baldwin, M. Bradley, Chem. Rev. 90 (1990) 1079–1088.
[20] D.M. Kurtz Jr, Chem. Rev. 90 (1990) 585–606.
[21] J. Du Bois, T.J. Mizoguchi, S.J. Lippard, Coord. Chem. Rev. 200 (2000) 443–485.
[22] S.P. de Visser, D. Kumar, S. Cohen, R. Shacham, S. Shaik, J. Am. Chem. Soc. 126 (2004) 8362–8363.
[23] S.P. de Visser, J. Am. Chem. Soc. 132 (2010) 1087–1097.
[24] S.P. de Visser, J. Am. Chem. Soc. 128 (2006) 15809–15818.
[25] J.C. Price, E.W. Barr, B. Tirupati, J.M. Bollinger, C. Krebs, Biochemistry 42 (2003) 7497–7508.
[26] W. Nam, Acc. Chem. Res. 40 (2007) 522–531.
[27] A. Ansari, A. Kaushik, G. Rajaraman, J. Am. Chem. Soc. 135 (2013) 4235–4249.
[28] O.V. Makhlynets, P. Das, S. Taktak, M. Flook, R. Mas-Balleste, E.V. Rybak-Akimova, L. Que Jr., Chem. Eur. J. 15 (2009) 13171–13180.
[29] S. Taktak, M. Flook, B.M. Foxman, L. Que Jr., E.V. Rybak-Akimova, Chem. Commun. (2005) 5301–5303.
[30] A. Ansari, G. Rajaraman, Phys. Chem. Chem. Phys. 16 (2014) 14601–14613.
[31] O.V. Makhlynets, E.V. Rybak-Akimova, Chem. Eur. J. 16 (2010) 13995–14006.
[32] M.L. Matthews, C.M. Krest, E.W. Barr, F.H. Vaillancourt, C.T. Walsh, M.T. Green, C. Krebs, J.M. Bollinger Jr, Biochemistry 48 (2009) 4331–4343.
[33] D. Galonić Fujimori, E.W. Barr, M.L. Matthews, G.M. Koch, J.R. Yonce, C.T. Walsh, J.M. Bollinger Jr, C. Krebs, P.J. Riggs-Gelasco, J. Am. Chem. Soc. 129 (2007) 13408–13409.
[34] D.P. Galonić, E.W. Barr, C.T. Walsh, J.M. Bollinger Jr, C. Krebs, Nat. Chem. Biol. 3 (2007) 113–116.
[35] T. Borowski, H. Noack, M. Radon, K. Zych, P.E. Siegbahn, J. Am. Chem. Soc. 132 (2010) 12887–12898.
[36] S.P. de Visser, R. Latifi, J. Phys. Chem. B 113 (2009) 12–14.
[37] M.G. Quesne, S.P. de Visser, J. Biol. Inorg. Chem. 17 (2012) 841–852.
[38] P. Comba, S. Wunderlich, Chem. Eur. J. 16 (2010) 7293–7299.
[39] M. Puri, A.N. Biswas, R. Fan, Y. Guo, L. Que Jr., J. Am. Chem. Soc. 138 (2016) 2484–2487.
[40] S. Chatterjee, T.K. Paine, Angew. Chem. Int. Ed. 55 (2016) 7717–7722.
[41] S. Rana, J.P. Biswas, A. Sen, M. Clémancey, G. Blondin, J.-M. Latour, G. Rajaraman, D. Maiti, Chem. Sci. 9 (2018) 7843–7858.
[42] M.L. Matthews, W.-C. Chang, A.P. Layne, L.A. Miles, C. Krebs, J.M. Bollinger Jr, Nat. Chem. Biol. 10 (2014) 209–215.
[43] F.H. Vaillancourt, E. Yeh, D.A. Vosburg, S. Garneau-Tsodikova, C.T. Walsh, Chem. Rev. 106 (2006) 3364–3378.
[44] D. Kumar, G.N. Sastry, S.P. De Visser, Chem. Eur. J. 17 (2011) 6196–6205.
[45] C.V. Sastri, M.J. Park, T. Ohta, T.A. Jackson, A. Stubna, M.S. Seo, J. Lee, J. Kim, T. Kitagawa, E. Münck, J. Am. Chem. Soc. 127 (2005) 12494–12495.
[46] R. Kumar, A. Ansari, G. Rajaraman, Chem. Eur. J. 24 (2018) 6818–6827.
[47] S.P. de Visser, J. Biol. Inorg. Chem. 11 (2006) 168–178.
[48] L. Bernasconi, M.J. Louwerse, E.J. Baerends, Eur. J. Inorg. Chem. (2007) 3023–3033.
[49] S.A. Wilson, J. Chen, S. Hong, Y.-M. Lee, M. Clémancey, R. Garcia-Serres, T. Nomura, T. Ogura, J.-M. Latour, B. Hedman, J. Am. Chem. Soc. 134 (2012) (1806) 11791–11799.
[50] S. Shaik, D. Danovich, A. Fiedler, D. Schroeder, H. Schwarz, Helv. Chim. Acta 78 (1995) 1393–1407.
[51] C. Geng, S. Ye, F. Neese, Dalton Trans. 43 (2014) 6079–6086.
[52] T. Matsuo, J.M. Mayer, Inorg. Chem. 44 (2005) 2150.
[53] A. Bassan, M.R.A. Blomberg, P.E.M. Siegbahn, L. Que Jr., J. Am. Chem. Soc. 124 (2002) 11056–11063.
[54] H. Chen, W. Lai, J. Yao, S. Shaik, J. Chem. Theory Comput. 7 (2011) 3049–3053.
[55] A. Chanda, X. Shan, M. Chakrabarti, W.C. Ellis, D.L. Popescu, F. Tiago de Oliveira, D. Wang, L. Que Jr., T.J. Collins, E. Münck, Inorg. Chem. 47 (2008) 3669–3678.
[56] S. Kundu, J.V.K. Thompson, L.Q. Shen, M.R. Mills, E.L. Bominaar, A.D. Ryabov, T. J. Collins, Chem. Eur. J. 21 (2015) 1803–1810.
[57] K.K. Singh, M.k. Tiwari, B.B. Dhar, K. Vanka, S. Sen Gupta, Inorg. Chem. 54 (2015) 6112–6121.
[58] M. Ghosh, K.K. Singh, C. Panda, A. Weitz, M.P. Hendrich, T.J. Collins, B.B. Dhar, S. Sen Gupta, J. Am. Chem. Soc. 136 (2014) 9524–9527.
[59] R. Fan, J. Serrano-Plana, W.N. Oloo, A. Draksharapu, E. Delgado-Pinar, A. Company, V. Martin-Diaconescu, M. Borrell, J. Lloret-Fillol, E. García-España, Y. Guo, E.L. Bominaar, L. Que Jr., M. Costas, E. Münck, J. Am. Chem. Soc. 140 (2018) 3916–3928.

[60] J. Serrano-Plana, W.N. Oloo, L. Acosta-Rueda, K.K. Meier, B. Verdejo, E. García-España, M.G. Basallote, E. Münck, L. Que Jr., A. Company, J. Am. Chem. Soc. 137 (2015) 15833–15842.
[61] K.B. Cho, Y. Moreau, D. Kumar, D.A. Rock, J.P. Jones, S. Shaik, Chem. Eur. J. 13 (2007) 4103–4115.
[62] F.P. Guengerich, C.-H. Yun, T.L. Macdonald, J. Biol. Chem. 271 (1996) 27321–27329.
[63] A. Lennartson, C.J. McKenzie, Angew. Chem. Int. Ed. 51 (2012) 6767–6770.
[64] C. Wegeberg, C.G. Frankær, C.J. McKenzie, Dalton Trans. 45 (2016) 17714–17722.
[65] Y. Kang, X.-X. Li, K.-B. Cho, W. Sun, C. Xia, W. Nam, Y. Wang, J. Am. Chem. Soc. 139 (2017) 7444–7447.
[66] B. Wang, Y.M. Lee, M.S. Seo, W. Nam, Angew. Chem. Int. Ed. 54 (2015) 11740–11744.
[67] R. Kumar, B. Pandey, G. Rajaraman, J. Indian Chem. Soc. 96 (2019) 825–836.
[68] X. Engelmann, I. Monte-Pérez, K. Ray, Angew. Chem. Int. Ed. 55 (2016) 7632–7649.
[69] M. Guo, T. Corona, K. Ray, W. Nam, ACS Cent Sci. 5 (2018) 13–28.
[70] L. Roy, ChemPlusChem 84 (2019) 893–906.
[71] J.T. Groves, Proc. Natl. Acad. Sci. USA 100 (2003) 3569–3574.
[72] F.P. Guengerich, Chem. Res. Toxicol. 14 (2001) 611–650.
[73] M. Sono, M.P. Roach, E.D. Coulter, J.H. Dawson, Chem. Rev. 96 (1996) 2841–2888.
[74] T.L. Poulos, J. Biol. Inorg. Chem. 1 (1996) 356–359.
[75] J.H. Dawson, R.H. Holm, J.R. Trudell, G. Barth, R.E. Linder, E. Bunnenberg, C. Djerassi, S.C. Tang, J. Am. Chem. Soc. 98 (1976) 3707–3709.
[76] A. Dey, Y. Jiang, P. Ortiz de Montellano, K.O. Hodgson, B. Hedman, E.I. Solomon, J. Am. Chem. Soc. 131 (2009) 7869–7878.
[77] W.-D. Woggon, Acc. Chem. Res. 38 (2005) 127–136.
[78] M.T. Green, J.H. Dawson, H.B. Gray, Science 304 (2004) 1653–1656.
[79] F. Ogliaro, S.P. de Visser, S. Shaik, J. Inorg. Biochem. 91 (2002) 554–567.
[80] J.H. Dawson, Science 240 (1988) 433–439.
[81] J.T. Groves, R.C. Haushalter, M. Nakamura, T.E. Nemo, B. Evans, J. Am. Chem. Soc. 103 (1981) 2884–2886.
[82] J.T. Groves, T.E. Nemo, R.S. Myers, J. Am. Chem. Soc. 101 (1979) 1032–1033.
[83] H. Fujii, Coord. Chem. Rev. 226 (2002) 51–60.
[84] J.-U. Rohde, J.-H. In, M.H. Lim, W.W. Brennessel, M.R. Bukowski, A. Stubna, E. Münck, W. Nam, L. Que Jr., Science 299 (2003) 1037–1039.
[85] V. Balland, M.F. Charlot, F. Banse, J.J. Girerd, T.A. Mattioli, E. Bill, J.F. Bartoli, P. Battioni, D. Mansuy, Eur. J. Inorg. Chem. 2004 (2004) 301–308.
[86] M.H. Lim, J.-U. Rohde, A. Stubna, M.R. Bukowski, M. Costas, R.Y.N. Ho, E. Munck, W. Nam, L. Que Jr., Proc. Natl. Acad. Sci. USA 100 (2003) 3665–3670.
[87] J. Kaizer, E.J. Klinker, N.Y. Oh, J.-U. Rohde, W.J. Song, A. Stubna, J. Kim, E. Münck, W. Nam, L. Que Jr., J. Am. Chem. Soc. 126 (2004) 472–473.
[88] S. Meyer, I. Klawitter, S. Demeshko, E. Bill, F. Meyer, Angew. Chem. Int. Ed. 52 (2013) 901–905.
[89] Z. Gross, S. Nimri, Inorg. Chem. 33 (1994) 1731–1732.
[90] A. Takahashi, D. Yamaki, K. Ikemura, T. Kurahashi, T. Ogura, M. Hada, H. Fujii, Inorg. Chem. 51 (2012) 7296–7305.
[91] W.J. Song, Y.O. Ryu, R. Song, W. Nam, J. Biol. Inorg. Chem. 10 (2005) 294–304.
[92] J.U. Rohde, L. Que Jr., Angew. Chem. Int. Ed. 44 (2005) 2255–2258.
[93] A. Decker, J.-U. Rohde, L. Que Jr., E.I. Solomon, J. Am. Chem. Soc. 126 (2004) 5378–5379.
[94] C.V. Sastri, J. Lee, K. Oh, Y.J. Lee, J. Lee, T.A. Jackson, K. Ray, H. Hirao, W. Shin, J. A. Halfen, Proc. Natl. Acad. Sci. USA 104 (2007) 19181–19186.
[95] J. England, J.O. Bigelow, K.M. Van Heuvelen, E.R. Farquhar, M. Martinho, K.K. Meier, J.R. Frisch, E. Münck, L. Que Jr., Chem. Sci. 5 (2014) 1204–1215.
[96] D. Mandal, R. Ramanan, D. Usharani, D. Janardanan, B. Wang, S. Shaik, J. Am. Chem. Soc. 137 (2015) 722–733.
[97] X. Sun, C. Geng, R. Huo, U. Ryde, Y. Bu, J. Li, J. Phys. Chem. B 118 (2014) 1493–1500.
[98] C. Geng, S. Ye, F. Neese, Angew. Chem. Int. Ed. 49 (2010) 5717–5720.
[99] S. Hong, H. So, H. Yoon, K.-B. Cho, Y.-M. Lee, S. Fukuzumi, W. Nam, Dalton Trans. 42 (2013) 7842–7845.
[100] S. Hong, Y.-M. Lee, K.-B. Cho, K. Sundaravel, J. Cho, M.J. Kim, W. Shin, W. Nam, Chem. Soc. 133 (2011) 11876–11879.
[101] S. Ye, C. Kupper, S. Meyer, E. Andris, R. Navratil, O. Krahe, B. Mondal, M. Atanasov, E. Bill, J. Roithova, J. Am. Chem. Soc. 138 (2016) 14312–14325.
[102] F.G. Cantú Reinhard, S.P. de Visser, Chem. Eur. J. 23 (2017) 2935–2944.
[103] C. Kupper, B. Mondal, J. Serrano-Plana, I. Klawitter, F. Neese, M. Costas, S. Ye, F. Meyer, J. Am. Chem. Soc. 139 (2017) 8939–8949.
[104] K. Mittra, M.T. Green, J. Am. Chem. Soc. 141 (2019) 5504–5510.
[105] X. Wang, R. Ullrich, M. Hofrichter, J.T. Groves, Proc. Natl. Acad. Sci. U.S.A. 112 (2015) 3686–3691.
[106] J.M. Mayer, Acc. Chem. Res. 31 (1998) 441–450.
[107] X. Lu, X.-X. Li, M.S. Seo, Y.-M. Lee, M. Clémancey, P. Maldivi, J.-M. Latour, R. Sarangi, S. Fukuzumi, W. Nam, J. Am. Chem. Soc. 141 (2019) 80–83.
[108] X. Huang, J.T. Groves, Chem. Rev. 118 (2017) 2491–2553.
[109] E.L. Onderko, A. Silakov, T.H. Yosca, M.T. Green, Nat. Chem. 9 (2017) 623–628.
[110] D. Wang, K. Ray, M.J. Collins, E.R. Farquhar, J.R. Frisch, L. Gómez, T.A. Jackson, M. Kerscher, A. Waleska, P. Comba, Chem. Sci. 4 (2013) 282–291.
[111] G. Mukherjee, C.W. Lee, S.S. Nag, A. Alili, F.G.C. Reinhard, D. Kumar, C.V. Sastri, S.P. de Visser, Dalton Trans. 47 (2018) 14945–14957.
[112] G. Mukherjee, A. Alili, P. Barman, D. Kumar, C.V. Sastri, S.P. de Visser, Chem. Eur. J. 25 (2019) 5086–5098.
[113] W. Rasheed, A. Draksharapu, S. Banerjee, V.G. Young Jr, R. Fan, Y. Guo, M. Ozerov, J. Nehrkorn, J. Krzystek, J. Telser, L. Que Jr., Angew. Chem. Int. Ed. 57 (2018) 9387–9391.
[114] I. Grgurina, A. Barca, S. Cervigni, M. Gallo, A. Scaloni, P. Pucci, Experientia 50 (1994) 130–133.
[115] C.M. Harris, R. Kannan, H. Kopecka, T.M. Harris, J. Am. Chem. Soc. 107 (1985) 6652–6658.
[116] F.H. Vaillancourt, E. Yeh, D.A. Vosburg, S.E. O'Connor, C.T. Walsh, Nature 436 (2005) 1191–1194.
[117] J.C. Price, E.W. Barr, T.E. Glass, C. Krebs, J.M. Bollinger, J. Am. Chem. Soc. 125 (2003) 13008–13009.
[118] L.M. Hoffart, E.W. Barr, R.B. Guyer, J.M. Bollinger, C. Krebs, Proc. Natl. Acad. Sci. U.S.A. 103 (2006) 14738–14743.
[119] S. Pandian, M.A. Vincent, I.H. Hillier, N.A. Burton, Dalton Trans. (2009) 6201–6207.
[120] H. Noack, P.E. Siegbahn, J. Biol. Inorg. Chem. 12 (2007) 1151–1162.
[121] D. Kumar, H. Hirao, L. Que Jr., S. Shaik, J. Am. Chem. Soc. 127 (2005) 8026–8027.
[122] P.K. Sydor, S.M. Barry, O.M. Odulate, F. Barona-Gomez, S.W. Haynes, C. Corre, L. Song, G.L. Challis, Nat. Chem. 3 (2011) 388–392.
[123] M. Costas, M.P. Mehn, M.P. Jensen, L. Que Jr., Chem. Rev. 104 (2004) 939–986.
[124] M.P. Jensen, M.P. Mehn, L. Que Jr., Angew. Chem., Int. Ed. 42 (2003) 4357–4360.
[125] E.J. Klinker, T.A. Jackson, M.P. Jensen, A. Stubna, G. Juhasz, E.L. Bominaar, E. Muenck, L. Que Jr., Angew. Chem., Int. Ed. 45 (2006) 7394–7397.
[126] M. Jaccob, G. Rajaraman, Dalton Trans. 41 (2012) 10430–10439.
[127] A.K. Vardhaman, P. Barman, S. Kumar, C.V. Sastri, D. Kumar, S.P. de Visser, Angew. Chem. Int. Ed. 52 (2013) 12288–12292.
[128] S.P. de Visser, K. Oh, A.R. Han, W. Nam, Inorg. Chem. 46 (2007) 4632–4641.
[129] S. Kumar, A.S. Faponle, P. Barman, A.K. Vardhaman, C.V. Sastri, D. Kumar, S.P. de Visser, J. Am. Chem. Soc. 136 (2014) 17102–17115.
[130] B. Pandey, M. Jaccob, G. Rajaraman, Chem. Commun. 53 (2017) 3193–3196.